Marine Structures 75 (2021) 102850

Contents lists available at ScienceDirect

Marine Structures

journal homepage: http://www.elsevier.com/locate/marstruc

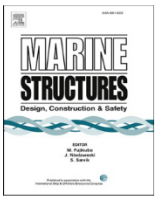

Glacial ice impacts: Part I: Wave-driven motion and small glacial ice feature impacts

Wenjun Lu [a,b,c,*], Jørgen Amdahl [d,e], Raed Lubbad [a,b], Zhaolong Yu [d,e], Sveinung Løset [a,b]

[a] ArcISo AS, Trondheim, Norway
[b] Sustainable Arctic Marine and Coastal Technology (SAMCoT), Norwegian University of Science and Technology (NTNU), Norway
[c] The Norwegian Academy of Science and Letters DNVA, Oslo, Norway
[d] Department of Marine Technology, Norwegian University of Science and Technology (NTNU), Norway
[e] Center for Autonomous Marine Operations and Systems (AMOS), Norwegian University of Science and Technology (NTNU), Norway

ARTICLE INFO

Keywords:
Glacial ice
Impacts
Wave driven motion
Froude-krylov force
Nonlinear hydrodynamic effects

ABSTRACT

Glacial ice features in the northern and central Barents Sea may threaten ships and offshore structures. Particularly, small glacial ice features, which are difficult to detect and manage by concurrent technologies, are of concern. Additionally, small glacial ice features are more susceptible to wave-driven oscillatory motions, which increases their pre-impact kinetic energy and may damage ships and offshore structures. This paper is part of three related papers. An initial paper (Monteban et al., 2020) studied glacial ice features' drift, size distribution and encounter frequencies with an offshore structure in the Barents Sea. The following two papers (Paper I and Paper II) further performed glacial ice impact studies, including impact motion analysis (Paper I) and structural damage assessment (Paper II). This paper (Paper I) studies the wave-driven motion of small glacial ice features and their subsequent impact with a given offshore structure. The aim here is to develop a numerical model that is capable of efficiently calculating the relative motion between the ice feature and structure and to sample a sufficient amount of impact events from which statistical information can be obtained. The statistical information entails the distributions of the impact location and associated impact velocities. Given the distributions of the impact velocities at different locations, we can quantify the kinetic energy for related impact scenarios for a further structural damage assessment in Paper II (Yu et al., 2020).

In Paper I, a numerical model that separately calculates the wave-driven oscillatory motion and the mean drift motion of small glacial ice features is proposed, implemented and validated. Practical and fit-for-purpose hydrodynamic simplifications are made to simulate and sample sufficient impact events. The numerical model has been favourably validated against existing numerical results and experimental data. A case study is presented where a 10 m wide glacial ice feature is drifting under the influence of surface waves towards an offshore structure. The case study shows that if an impact happens, the overall impact location and impact velocity can be best fitted by the Normal and Weibull distributions, respectively. Additionally, the impact velocity increases with impact height. Moreover, the impact velocity increases and the impact range is more dispersed in a higher sea state. It is also important to notice that the approaches and methods proposed in this paper adhere to and reflect the general requirements stated in ISO19906

* Corresponding author. ArcISo AS, Trondheim, Norway.
E-mail address: wenjun.lu@ntnu.no (W. Lu).

https://doi.org/10.1016/j.marstruc.2020.102850
Received 2 April 2020; Received in revised form 26 June 2020; Accepted 27 August 2020
Available online 22 September 2020
0951-8339/© 2020 The Authors. Published by Elsevier Ltd. This is an open access article under the CC BY license (http://creativecommons.org/licenses/by/4.0/).

(2019) and NORSOK N-003 (2017) for estimating the design kinetic energy for glacial ice impacts.

1. Introduction

Glacial ice may pose a significant impact hazard to ships and offshore structures in northern waters, such as the Barents Sea. A recent study by Monteban et al. [1] indicates that glacial ice features of smaller sizes in the Barents Sea are greater than originally anticipated by previous studies (e.g., from the Ice Data Acquisition Program [4,5]), which has a consequence on the design and operation of Arctic offshore structures. Due to the presence of drifting glacial ice features (e.g., icebergs), ice management is needed to safely operate most Arctic offshore structures [6,7]. For the ice management system to be able to respond to an incoming glacial ice feature that is on a collision course, the first step is to detect these features [8]. However, the detection of small glacial ice features is difficult as previously reported [9,10]. Additionally, small glacial ice features are more susceptible to wave-driven motions, i.e., both oscillatory and drift motions. Despite the small mass of these glacial ice features, their wave-driven motion can still induce a significant amount of kinetic energy that will be available for impact. However, most previous studies were mainly focused on the impact of large glacial ice features (i.e., icebergs), for which the wave-driven motion (particularly the oscillatory motion) is negligible; thus, only wind, wave and/or current-driven drift motion are utilised to derive the impact probability and velocities. This paper seeks to fill this gap by studying the impact from a small glacial ice feature whose motion (both oscillatory and drift) is driven by waves.

The kinetic energy of an approaching glacial ice feature is of concern for the considered impact design. The relative motions between the glacial ice feature and structure determine 1) whether there will be collision or not; and 2) how much kinetic energy is associated with the collision. The above two questions can be resolved by quantifying 1) the trajectory; 2) the added mass; and 3) the impact velocity of the drifting glacial ice feature.

The simplest approach to quantifying these parameters is through far-field drift modelling according to the classification by Sayeed et al. [11]. The idea is to equate the drift velocity to the impact velocity. The modelling considers the drag forces from wind and current and other force terms (e.g., Coriolis force and influence from the wave slopes). The wave forcing terms are not often included in these models, e.g., the models by Mountain [12] and by Sodhi and El-Tahan [13]; alternatively, only the wave-driven drift/linear motion is included but not the oscillatory motion, e.g., related models in the literature [14–16]. These modelling approaches are mainly for large icebergs and cover a rather large geophysical and temporal span. To perform such a large-scale drift simulation, many aspects of a glacial ice feature's hydrodynamic behaviours are simplified.

A more detailed formulation requires the inclusion of the wave-induced oscillatory motion of glacial ice features to derive the corresponding added mass and impact velocities. Most of the related theoretical models are based on the linear potential theory [17,18]. Together with related model tests [19], it was concluded that wave-induced oscillatory motion is important for the calculation of the impact velocity, particularly for small glacial ice features. Recent studies focusing on the wave induced motions of small glacial ice features [20–22] also confirm this result. However, all the previous theoretical studies are based on linear wave theories and do not consider the nonlinearities of small glacial ice features in waves, such as the two-body hydrodynamic effects and submergence.

It is acknowledged that a glacial ice feature's motion is influenced by the presence of an offshore structure. However, the direction (i.e., conservative or less conservative) and degree of such influences on the kinetic energy of the impact are not clear. Based on potential theory analyses, the added mass of a glacial ice feature increases with decreasing distance (gap) between the ice and structure. A comparison with the far-field added mass shows that the near-structure added mass experiences a 10% increase in the sway direction for large icebergs [23] and 47% increase in the sway direction for small glacial ice features [24]. The model by Isaacson and Stritto [23] shows that for small glacial ice features, both the oscillatory and drift velocities are reduced with decreasing distance between the ice and structure, whereas for medium size glacial ice features, only the drift velocity is reduced while the oscillatory motion is only minimally influenced by its distance from the structure. Isaacson and McTaggart [25] observed a similar drift velocity reduction (approximately 10%) with decreasing distance between the ice and structure. Most of the preceding studies are based on the potential theory, in which errors and/or numerical instabilities arise when the gap between the two bodies gets smaller [26,27]. Further physical model tests highlight the mismatch between theoretical/numerical predictions and laboratory measurements while the gap between two floating bodies decreases; and this is attribute to the lack of viscous effect in previous models [28]. Apparently, accounting for the detailed hydrodynamic interaction between the two bodies is rather challenging, both theoretically and computationally. Moreover, the influence of distance-dependent hydrodynamic coefficients on the kinetic energy is not straightforward. This is to say, as the ice approaches the structure, its added mass can increase, whereas the impact velocity is reported to decrease in most studies. How would the combined effect, i.e., the kinetic energy, be influenced? Given the immature research status, McTaggart (1989) suggests that "*hydrodynamic interactions between a structure and approaching icebergs can be neglected when designing for iceberg collisions in most cases (p.227)*".

Instead of devoting our research effort to studying the detailed hydrodynamic interactions between a glacial ice feature and a structure using computational methods (e.g., computational fluid dynamics) to solve a yet-unknown suitable turbulence model in a case-by-case scenario, we will perform practical and fit-for-purpose hydrodynamic simplifications in this paper to obtain more general results that target the derivation of the design kinetic energy, which often requires a large amount of repeated simulations. The context of these simplifications is descried in the research problem statement (Section 2). Subsequently, the theoretical formulation of the numerical model and its validations are presented in Section 3. Then, a case study of a 10 m wide glacial ice feature's impact with a given structure is carried out in Section 4; and the results, discussions and conclusions are presented in Sections 5 and 7, respectively.

2. Research problem statement

2.1. Designed kinetic energy

According to the NORSOK N-003 [29]; the probability of an impact between a glacial ice feature and a platform is estimated as a part of the design process prior to operations in the Barents Sea. We suggest using the kinetic energy E_k^V of a glacial ice feature as the 'ice action'. This value is conveniently used as the input value for a structural damage assessment (see e.g., Paper II [2]). During the impact, a substantial part of the E_k^V is dissipated by structural and ice deformation. For an individual impact action, E_k^V is formulated in Eq. (1),

$$E_k^V = \frac{1}{2}(M+A)\left(V_{impact}\right)^2 \tag{1}$$

where M and A are the mass and added mass of a given glacial ice feature; and V_{impact} is the impact velocity, which depends on the mean drift velocity as well as the wave induced oscillatory velocity. In Eq. (1), the statistical distribution of M is site specific. The distribution of mass and geometry and the encounter frequency E_N can be obtained either from credible field measurements or from far-field simulations [30]. With a known statistical distribution of M and A and the derived distribution of V_{impact}, the cumulative distribution function $F_V(E_k)$ of individual ice actions can be established.

According to ISO19906 [3]; the design kinetic energy E_k^{design} corresponding to the extreme level (EL, 10^{-2}) and abnormal level (AL, e.g., 10^{-4}) are presented in Eqs. (3) and (4) with subscripts 'E' and 'A', respectively. The cumulative distribution function $F_Z(E_k)$ of the annual maxima E_k^Z can be related to the cumulative distribution function $F_V(E_k)$ of ice actions through Eq. (2) with known encounter frequency E_N.

$$F_Z(E_k) = \exp\{-E_N[1-F_V(E_k)]\} \tag{2}$$

$$F_Z\left(E_{k,E}^{design}\right) = 0.99 \tag{3}$$

$$\begin{aligned} F_Z\left(E_{k,A}^{design}\right) &= 0.9999 \text{ (for L1 structures)} \\ &= 0.999 \quad \text{(for L2 structures)} \end{aligned} \tag{4}$$

2.2. Small glacial ice features' motions in waves

The previous section shows that we need to know the impact velocity V_{impact} of glacial ice features of various sizes (e.g., various $(M+A)$) to construct the needed kinetic energy distributions. Given the potentially large amount of small glacial ice features in the Barents Sea and their potential significant wave driven motions, this paper focused on the study of 'small' glacial ice features whose motions are heavily influenced by waves. Fig. 1 exemplified the possible motion characteristics for a small glacial ice feature (approximately 30 m) in waves. The motion exhibits nonlinearities (due to water flushing and submergence) and significant wave-driven motions (e.g., heave motion of approximately 6 m).

Coupling the wave-driven glacial ice features' motion with the platform's motion, we can derive the impact velocity, which can be used to calculate the kinetic energy in Eq. (1). However, to obtain the distribution of kinetic energy, i.e., $F_V(E_k)$, extensive impact

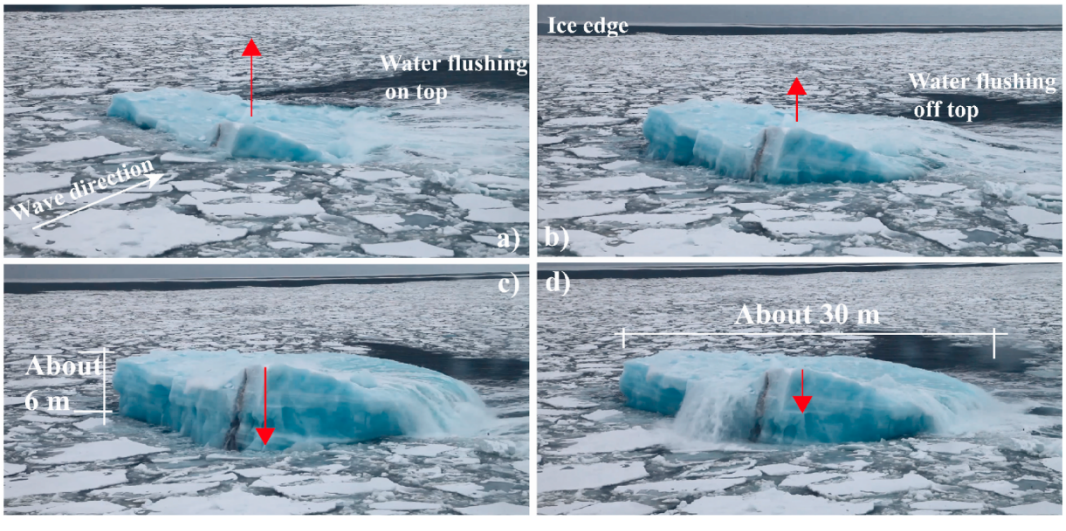

Fig. 1. Observed glacial ice features' motion in waves (filmed by Tsarau A. and Evgenii S. in 2015).

scenarios together with the distribution of impact velocities must be obtained. In this regard, we need to develop an efficient algorithm that can calculate the wave-driven motion of 'small' glacial ice features without sacrificing certain nonlinear features, such as submergence due to heave motion (typical for small glacial ice features as shown Fig. 1). Thereafter, enough impact scenarios and impact velocities should be efficiently sampled. This paper seeks to address these requirements by proposing, developing, and validating an efficient numerical model.

3. Method

To study and sample impact events between a glacial ice feature and a structure, we need to perform two tasks. First, the relative motion of the glacial ice feature and the structure should be analysed efficiently. Second, sampling of impact events (with both impact location and velocity) should be carried out efficiently. These two tasks are carried out sequentially in the proposed method.

Referring to Fig. 2, we define the origin of the coordinate system for each body at the Centre of Gravity (CoG) in still water. As this paper mainly focuses on obtaining statistical information of the glacial ice's impact locations and associated velocity on the structure, we adopt a practical and fit-for-purpose approach for hydrodynamic analyses where complex hydrodynamic interaction phenomena are neglected, which is consistent with previous research results and suggestions (e.g., by McTaggart (1989)). The motions of the glacial ice feature and the structure are calculated separately. As the size of the structure is quite large compared with its motion, linear wave theory is used to calculate its wave-driven motion. Nonlinearities concerning potential full submergence and slow drift force are considered for the small glacial ice feature.

3.1. Assumptions

A small glacial ice feature in waves experiences both oscillatory and drift motions. The following assumptions are made for the proposed numerical model.

- The oscillatory and drift motions can be decoupled.
- As shown in Fig. 2, we ignore the roll motion of the glacial ice feature and consider only two degrees-of-freedom (2 DOFs), i.e., in the sway ($i = 2$) and heave ($i = 3$) directions. As found by Ref. [31]; the rotational kinetic energy represents only 13% of the total kinetic energy, which is particularly so for small glacial ice features.
- The Froude-Krylov force component is calculated by integrating the incident wave pressure without considering the presence of the structure. Thus, the near-field hydrodynamic effects are not considered.
- Frequency-independent added mass and added damping coefficients are adopted.
- To calculate the wave diffraction force components, the long wave theory is adopted. This means that the ice body is 'transparent' in the wave field; and this assumption is valid when the characteristic body size (e.g., the breadth B of the ice body) and the wave length λ satisfy the relationship $\lambda/B > 5$ [32]. Considering the relatively limited size of the small glacial ice feature, this assumption is considered reasonable.

3.2. Wave-induced motion of the glacial ice feature

3.2.1. Oscillatory motion

For the wave induced oscillatory motion, the motion of a glacial ice feature may be described by Eq. (5):

$$(A_{ij} + M)\ddot{\eta}_i + B_{ij}\dot{\eta}_i = F_i^W + F_i^R \tag{5}$$

in which M is the mass of the glacial ice feature and η_i is the displacement of the glacial ice feature in i direction. We consider only 2 DOFs, i.e., in the sway ($i = 2$) and heave ($i = 3$) directions. The 'dot' represents a time derivative, which leads to $\ddot{\eta}_i$ and $\dot{\eta}_i$ being the acceleration and velocity, respectively. A_{ij} and B_{ij} are the constant added mass and added damping of the glacial ice feature, respectively. F_i^W is the wave excitation force; and F_i^R is the restoring force. To calculate the motion η of a glacial ice in waves, each force component is calculated as described below.

Because of the long wave assumption, i.e., the characteristic body size (e.g., the breadth B) and the wave length λ should satisfy the

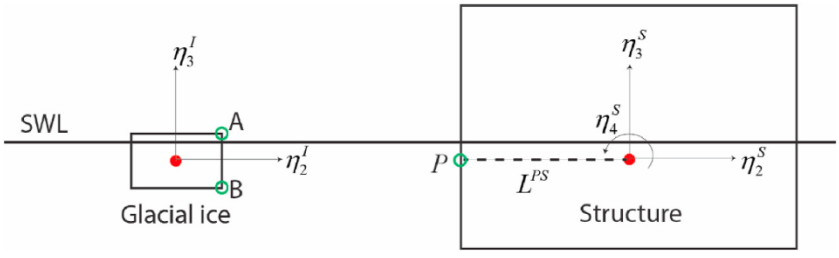

Fig. 2. Coordinate system of the studied problem (superscripts '*I*' and '*S*' represent glacial ice and structure, respectively).

relationship $\lambda/B > 5$[32]. We can write the generalised wave excitation force F^W as follows:

$$F_i^W = F_i^{FK} + F_i^{Diff} = -\iint_S p\mathbf{n_i} ds + A_{i1}a_1 + A_{i2}a_2 + A_{i3}a_3 \tag{6}$$

Eq. (6) shows that the wave excitation force consists of two parts: the Froude-Krylov force (see Eq. (7)) and the diffraction force (in Eq. (10)). In Eq. (7), ds is a panel of the instantaneous wetted surface of the ice feature S, p is the local pressure acting on ds, $\mathbf{n}$ is a unit vector on ds, and $\mathbf{n_i}$ is the component of $\mathbf{n}$ in the i direction. p can be calculated in Eq. (8) assuming an infinite water depth. The formulation in Eq. (8) is based on the incident wave pressure without considering the presence of the structure.

$$F_i^{FK} = -\iint_S p\mathbf{n_i} ds \tag{7}$$

$$p = \sum_{j=1}^{N} \begin{cases} \dfrac{\rho g \zeta_a^j}{\omega_j} e^{k_j z} \sin\left(\omega_j t - k_j x + \psi_j\right) & z \le 0 \\ \dfrac{\rho g \zeta_a^j}{\omega_j} \sin\left(\omega_j t - k_j x + \psi_j\right) & z > 0 \end{cases} \tag{8}$$

where $\rho = 1020\ \mathrm{kg/m^3}$ represents the water density; $g = 9.81\ \mathrm{m/s^2}$ represents the acceleration of gravity; ζ_a^j represents the wave amplitude of the jth wave component, in [m]; ω_j represents the circular frequency of the jth wave component, in [rad/s]; k_j represents the wave number and can be expressed as $k_j = 2\pi/\lambda_j$ for the jth wave component; ψ_j represents the phase angle uniformly distributed between 0 and 2π; and z represents the water depth calculated from the mean Still Water Level (SWL), and it is positive upward in [m] and expressed in Eq. (9). This parameter is solution dependent (i.e., depending on the instantaneous heave motion $\eta_3$and wave profile).

$$z = z_{SWL} + \eta_3 - \sum \zeta_a^j \sin\left(\omega_j t - k_j x + \psi_j\right) \tag{9}$$

where z_{SWL} is the vertical coordinate of the panel $ds$from the Still Water Level (SWL) when the floating body is in hydrostatic equilibrium.

For the general diffraction force expression F_i^{Diff} in Eq. (10), A_{22}, A_{33} are the added mass coefficients of the glacial ice feature in sway and heave directions, whereas a_2 and a_3 are the undisturbed fluid particle acceleration at the geometric centre of the wetted volume in the sway and heave directions, respectively [32]. They are expressed in Eq. (11).

$$F_i^{Diff} = A_{i2}a_2 + A_{i3}a_3 \tag{10}$$

$$\begin{aligned} a_2 &= \sum_{j=1}^{N} \omega_j^2 \zeta_a^j e^{k_j \bar{z}} \cos\left(\omega_j t - k_j x + \psi_j\right) \\ a_3 &= -\sum_{j=1}^{N} \omega_j^2 \zeta_a^j e^{k_j \bar{z}} \sin\left(\omega_j t - k_j x + \psi_j\right) \end{aligned} \tag{11}$$

where $\bar{z}$ is the vertical distance from the wetted volume centre to the SWL, and it is also solution dependent (i.e., depending on the heave motion η_3).

In Eq. (5), the restoring force F_i^R in the heave direction ($i = 3$) can be formulated as in Eq. (12), where $\mathbf{n_3}$ is a unit vector in the vertical direction positively upwards and $D(S)$ is the vertical distance from the centre of a wetted panel ds to the SWL, and it is expressed in Eq. (13).

$$F_3^R = \rho g \int D(s) ds \cdot \mathbf{n_3} - Mg \tag{12}$$

$$D(s) = z_{SWL}(s) - \eta_3 \tag{13}$$

In static equilibrium ($F_3^R = 0$) and the absence of vertical motion (i.e., $\eta_3 = 0$), Eq. (13) yields the following relation: $\rho g \int D(S) ds \cdot \mathbf{n_3} = Mg =$ wetted volume. In the special case of a cuboidal glacial ice feature, $\rho g \int D(S) ds \cdot \mathbf{n_3} = \rho g A_W \cdot$ draft, where A_W is the waterplane area of the cuboid. When the entire glacial ice feature is submerged, F_3^R becomes a constant (i.e., equal to the difference between the buoyancy and the gravity forces of the entire body).

Eqs. (5)–(12) are formulated in the time domain. The external forces, i.e., the wave excitation forces and restoring force, which are denoted overall as F_η on the right hand side of Eq. (5), are dependent on the instantaneous position η. The partial differential equation (PDE) system in Eq. (5) is solved with the explicit numerical scheme given by Eq. (14) [33].

$$\eta_{i,n+1} = \left(\frac{1}{\frac{M+A_{ii}}{\Delta t^2}+\frac{B_{ii}}{2\Delta t}}\right)\left[F(\eta_{i,n}) + \frac{2}{\Delta t^2}(M_{ii}+A_{ii})\eta_{i,n} - \left(\frac{M+A_{ii}}{\Delta t^2}-\frac{B_{ii}}{2\Delta t}\right)\eta_{n-1}\right] \quad (i=2,3) \tag{14}$$

where the subscript 'n' represents discrete stations in the time domain. The above formulations are implemented as MATLAB scripts, and the simulation yields the motion history $\eta_i(t)$of the glacial ice feature.

3.2.2. Slow drift motion

While evaluating the algorithm developed in Section 3.2.1, in addition to oscillatory motions, a horizontal 'slow drift motion' was also found in the solution of $\eta_2(t)$. However, this constitutes only a portion of the entire drift motion (more detailed proof is presented in Appendix A with Fig. 25). Any slow drift motion calculated by the formulation from Section 3.2.1 is filtered away, leaving only the oscillatory components. However, as the drift motion (either by wave, current or both) of a glacial ice feature is a necessity that leads to the occurrence of impact events [34,35], the wave-driven drift component is separately introduced here with the following assumptions:

- The oscillatory motion and slow drift motion can be decoupled;
- The floating glacial ice feature is always 'surface piercing', and the influence of nonlinear motions, such as total submergence, is excluded;
- The mean drift force is assumed to be balanced by the drag force, which is formulated with a constant wetted surface at the SWL and the mean drift velocity (see Eq. (17))

Given the above assumptions, the drift force for each regular wave frequency is calculated by Eq. (15), where the reflected wave height $A_R(\omega_j)$ is directly retrieved from Fig. 5.5 of Faltinsen [32].

$$\overline{F}_2(\omega_j) = \frac{\rho g}{2}A_R^2(\omega_j) \tag{15}$$

Although the theoretical curve in Fig. 5.5 of Faltinsen [32] is only for a width to draft ratio of 2 (i.e., $B/D = 2$), it is considered applicable to most glacial ice features whose geometric proportions follow the empirical relationship in Eq. (16) [36].

$$\begin{aligned} B &= 0.7L\exp(-0.00062L) \\ H &= 0.3L\exp(-0.00062L) \end{aligned} \tag{16}$$

where L, B and H are the length, breadth, and height of a glacial ice feature. These calculations give a typical breadth to draft ratio of $B/$

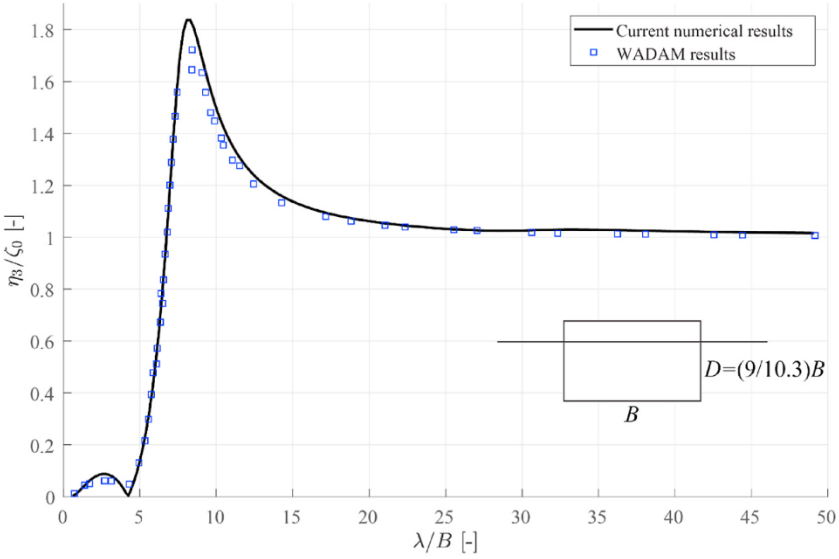

Fig. 3. Heave RAOs for the cuboidal glacial ice feature: comparison between WADAM and the current numerical results that exclude nonlinear effects using gentle regular wave conditions (i.e., low ζ_a/λ).

- Case #2: Lab-measured oscillatory motion in regular waves

$D = 2.63$, where $D \approx 0.9H$. Therefore, the results in Fig. 25 can be used to calculate the slow drift forces of most of the glacial ice features in regular waves, which will be validated in Section 3.2.3. For irregular wave conditions, the mean wave drift force is a linear summation of $\overline{F}_2(\omega_j)$ from each wave component [32]. Then, we can calculate the drift motion (i.e., mean drift velocity $\overline{V}_{drift}$) by simply equating the total mean drift force $\sum \overline{F}_2(\omega_j)$ with the drag force of Eq. (17).

$$\overline{F}_{drag} = \frac{1}{2} C_D \rho L D \overline{V}_{drift}^2 \tag{17}$$

Superimposing the oscillatory motion $\eta_i(t)$and the sway drift motion $\overline{V}_{drift} \cdot t$, the overall track of the glacial ice feature in waves is obtained.

3.2.3. Validation cases

In this section, we will validate the developed model against available numerical and experimental data concerning both the oscillatory and drift motion of glacial ice features in waves. Four cases of the validation are carried out.

- Case #1: Numerical simulated oscillatory motions based on linear wave theory

First, in a related study, Ekeberg et al. [20] performed frequency domain analyses of the Response Amplitude Operators (RAOs) for a cuboidal glacial ice feature using the commercial software - Wave Analysis by Diffraction and Morison theory (WADAM) [37].

The size of the cuboidal glacial ice features is length $L = 10$ m, breadth and height $B = H = 10.3$ m, and draft $D = 9.0$ m. In our numerical model, the motion was excited with regular waves with different frequencies with a rather gentle wave slope to avoid nonlinear effects, such as submergence. The RAOs for heave and sway are compared with the WADAM results in Fig. 3 and Fig. 4. For heave, the match is almost perfect; for the sway, the overall match is good except for the discrepancies in the range of $\lambda/B \approx [10, 30]$, which is believed to be due to the ignoring of the pitch motion in the current numerical model.

The overall agreement confirms the capability of the numerical model to reproduce results that are based on the linear wave theory, which is expected.

Lever et al. [19] performed model-scale tests regarding the motion of cubic glacial ice features in regular waves. The authors concluded that the measured results are consistent with linear RAOs despite the nonlinear behaviour, such as intermittent submergence and large excursions from the equilibrium. An overall comparison of their measured RAOs with the predictions of the current numerical model in regular waves is presented in Fig. 5 and Fig. 6, which show that simulations based on linear wave theory can capture most of the observed behaviour rather satisfactorily.

Lever et al. [19] conducted experiments with three different sized models of glacial ice features (i.e., small, medium and large ones). To obtain more insights, we simulated the exact wave conditions for the smallest glacial ice features. The results are compared in Fig. 7 and Fig. 8. In addition, the theoretical values from Lever et al. [19] are also presented.

Fig. 7 shows that the heave RAOs are consistent among all three methods when $\lambda/B > 15$; otherwise, the current numerical model underpredicts the heave motion compared to both the theoretical values and measurements. However, the current numerical model seems to yield results that are closer to the measurements than the theoretical values. In our simulations, constant submergence occurs

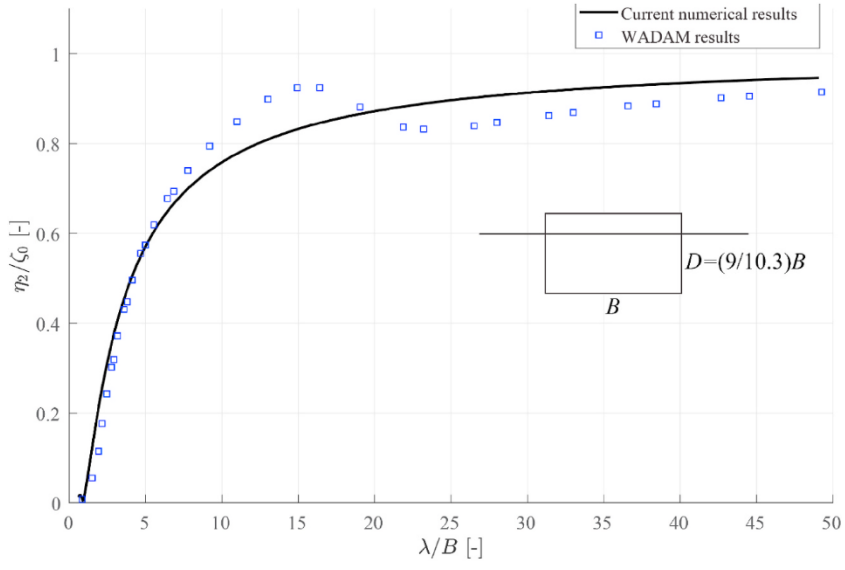

Fig. 4. Sway RAOs for the cuboidal glacial ice feature: comparison between WADAM and the current numerical results that exclude nonlinear effects using gentle regular wave conditions (i.e., low ζ_a/λ).

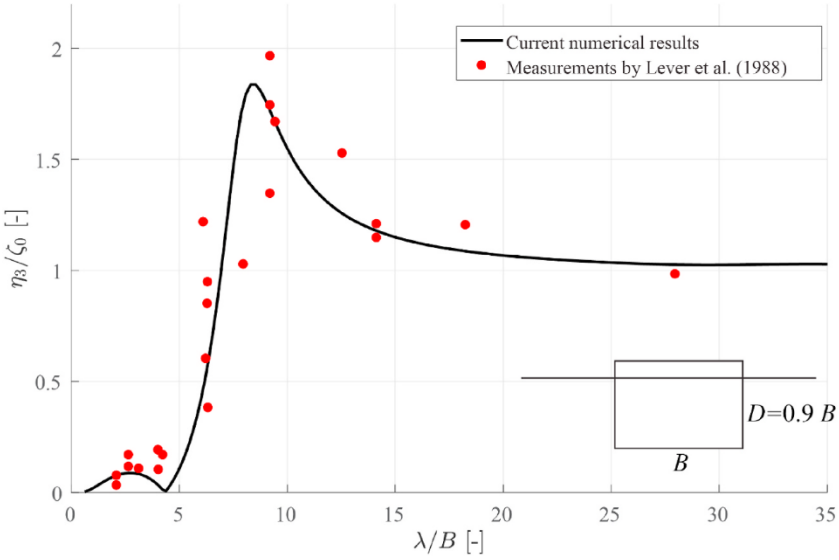

Fig. 5. Heave RAOs for cubic glacial ice feature: comparison between laboratory experiments and the current numerical results excluding nonlinear effects using gentle regular wave conditions (i.e., low ζ_a/λ).

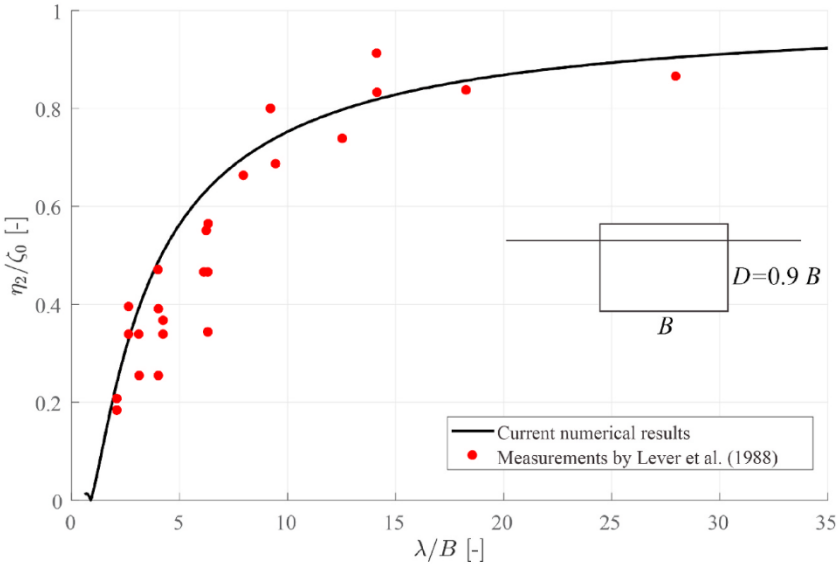

Fig. 6. Sway RAOs for cubic glacial ice feature: comparison between laboratory experiments and the current numerical results that exclude nonlinear effects using gentle regular wave conditions (i.e., low ζ_a/λ).

for the small glacial ice feature in regular waves with $\lambda/B = 6.30$, 8.02, and 12.60. Such nonlinearities are not included in the theoretical values in Fig. 7 (i.e., blue circles); and when submergence occurs, accurately measuring the motions may be difficult, which may explain the observed discrepancy.

Fig. 8 shows a comparison of the sway RAOs for the three different methods. A similar trend is observed. The current numerical model gives a much closer prediction to the measurements compared with the theoretical values. The theoretical values are based on the model originally developed by Sen [18]; which is based on linear potential theory and does not account for changes of the wetted surface. This inadequacy might explain the large discrepancy between predictions of the simplified model (i.e., blue circles), the measurements (red circles) and our numerical model (dark circles).

For long waves, the current numerical model gives satisfactory results, whereas for short waves, the accuracy is reduced compared to the measurements but better than that of the theoretical model based on linear wave theory and a constant wetted surface. Nonetheless, further validation under irregular wave conditions should be carried out to investigate its overall performance.

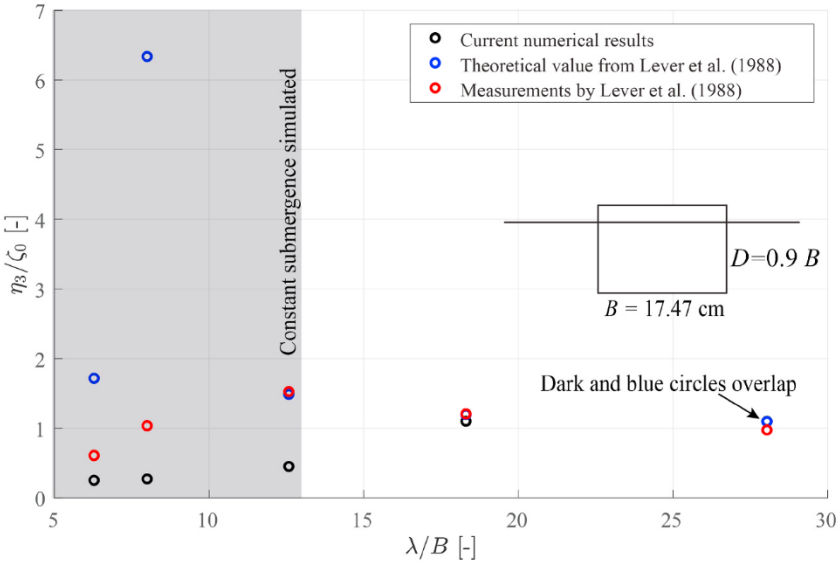

Fig. 7. Heave RAOs for the small cubic glacial ice feature: comparison among laboratory experiments (red circles), linear wave theory based results (blue circles), and the current numerical results (dark circles) that include nonlinear effects using the exact regular wave conditions (i.e., exact ζ_a and λ values). (For interpretation of the references to colour in this figure legend, the reader is referred to the Web version of this article.)

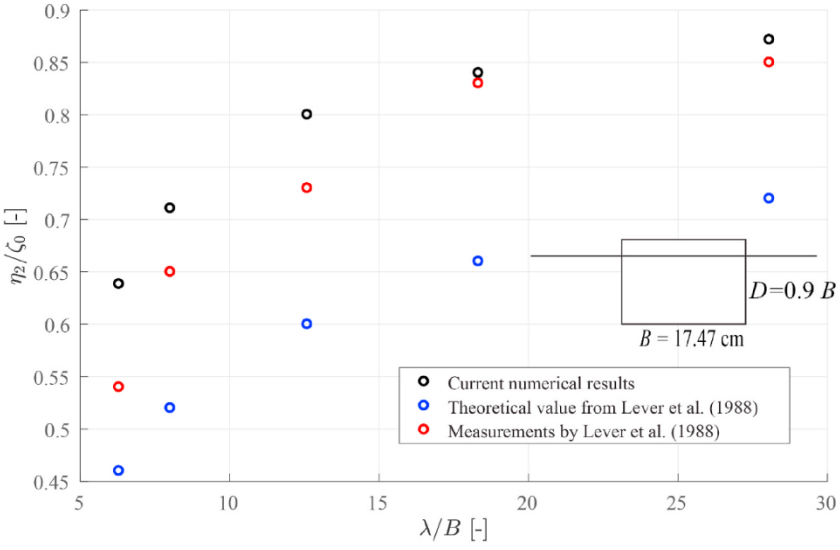

Fig. 8. Sway RAOs for the small cubic glacial ice feature: comparison among laboratory experiments (red circles), linear wave theory based results (blue circles), and the current numerical results (dark circles) that include nonlinear effects using the exact regular wave conditions (i.e., exact ζ_a and λ values). (For interpretation of the references to colour in this figure legend, the reader is referred to the Web version of this article.)

- Case #3: Field-measured oscillatory motion in irregular waves

Lever et al. [38] performed field experiments to measure the oscillatory motion of glacial ice features of varying sizes in irregular waves. The size of the glacial ice feature ranges from 3.30 m to 140 m; and the sea states were described by the JONSWAP wave spectrum with the measured significant wave height H_s, peak period T_P and corresponding peak wave length λ_p. Significant velocities in the sway (U_s) and heave (V_s) directions were estimated by means of Eq. (18).

$$U_s = 2\sqrt{\frac{\sum_{n=1}^{N}\left[\dot{\eta}_2(t_n) - \overline{\dot{\eta}_2(t_n)}\right]^2}{N-1}}, \quad V_s = 2\sqrt{\frac{\sum_{n=1}^{N}\left[\dot{\eta}_3(t_n) - \overline{\dot{\eta}_3(t_n)}\right]^2}{N-1}} \tag{18}$$

The significant velocities are presented in Fig. 9 and Fig. 10. The current numerical simulation results are repeated 30 times with different random samplings of the wave components and with different phase angles from the wave spectrum. When interpreting the comparisons, it should be noted that 1) the experiments were carried out on irregular glacial ice geometries; and 2) the measured results have an error range up to ±20% and ±40% for the significant velocities and ±10% and ±20% for the λ_P/B values [38]. The laboratory measurements [39] and the numerical simulations are based on cubic glacial ice features.

Given the above stated premises, the mutual agreement among the field and laboratory measurements and the current numerical results is encouraging. For the significant heave velocity (Fig. 9), the current numerical results fall well within the error ranges of the field measurements and laboratory measurements. It should be noted that the laboratory 'measurements' in Fig. 9 are obtained through motion calculations of the cubic glacial ice feature in the same JONSWAP wave spectrum with the RAOs measured in the laboratory. Therefore, it is a reflection of the linear wave theory [39]. It is highly probable that the discrepancies between the laboratory results (blue curve) and the numerical results (dark circles) are due to the inundation/submergence of the glacial ice features, which are neglected by the laboratory results (based on linear wave theory). The same trend is observed for the significant sway velocity (Fig. 10), i.e., the numerical results and the laboratory results are consistent for large λ_P/Bratios and also fall within the error range of the field measurements.

The agreement is encouraging and supports the application of the numerical model to predict the oscillatory motion of small glacial ice features in irregular wave conditions.

- Case #4: Wave-driven drift motion based on laboratory experiments

The calculation of wave-drive drift motion will be validated against laboratory experiments performed by Eik et al. [40]. Three cuboidal glacial ice features with different sizes were tested in various regular wave conditions. The drift velocity $\overline{V}_{drift}$, wave period T, and wave amplitude $\zeta_a$were measured. Using Eq. (17) to calculate the mean drift force $\overline{F_2}$ assuming $\overline{F_2} = \overline{F}_{drag}$ and using a drag coefficient $C_D = 0.9$according to Eik et al. [40]; we can plot the measured and the theoretical drift force as shown in Fig. 11.

Considering the experimental errors stated by Eik et al. [40] and scattering of the measurements, the comparison in Fig. 11 is considered satisfactory. In addition, we consider the theoretical curve more advantageous than the existing empirical formulas used to predict the drift motion of small glacial ice features (where $\omega\sqrt{D/g}$ becomes small) because most, if not all, of the existing empirical formulas were mainly developed for large glacial ice features.

3.2.4. *Summary of the validations*

Table 1 summarises all the validation cases' results and the goodness of fitting in terms of the calculated R-squared values (i.e., R^2). Most of the R-squared values are larger than 0.7 signifying reasonable agreements between the current numerical prediction with existing numerical and experimental results. The low R-squared value for Fig. 7 (i.e., $R^2 = 0.0068$) is mainly because of the discrepancies in the first three data points (among all five data points), which are explained as the nonlinear inundation/submergence process in the shaded area in Fig. 7. In addition, the R-squared values are not presented for the validations in Case #3. This is because the field measurements involve different glacial ice geometries and relatively larger measurement errors. Moreover, it is not our intention to fit our simulation with idealised geometries with these data. Instead, as illustrated in Figs. 9 and 10, these two data set are

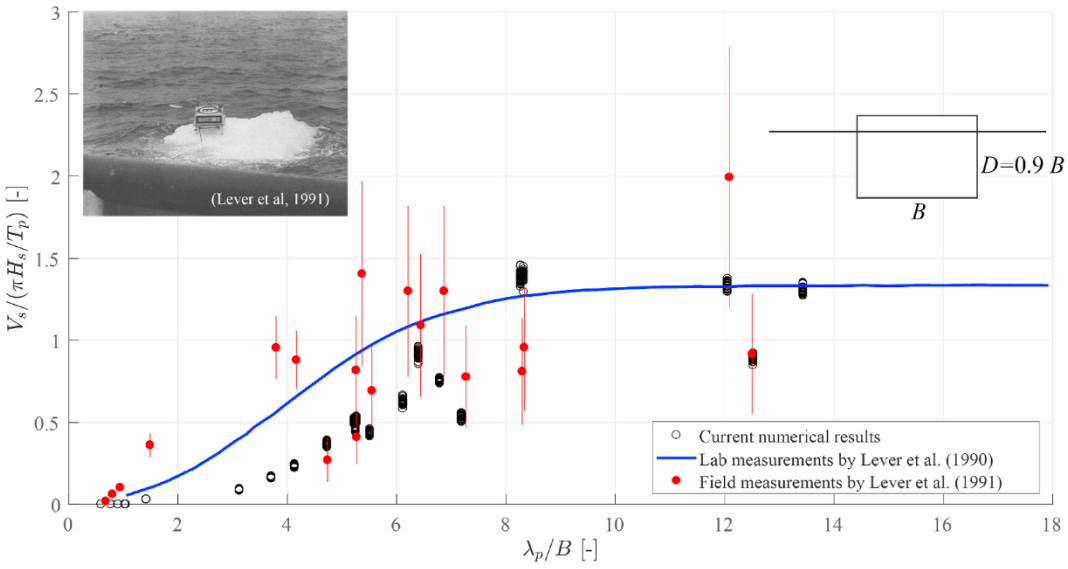

Fig. 9. Comparison of significant heave velocities for various sized glacial ice feature in various irregular wave conditions described by the JONSWAP wave spectrum with significant wave height H_s, peak wave period T_P and peak wave length λ_P.

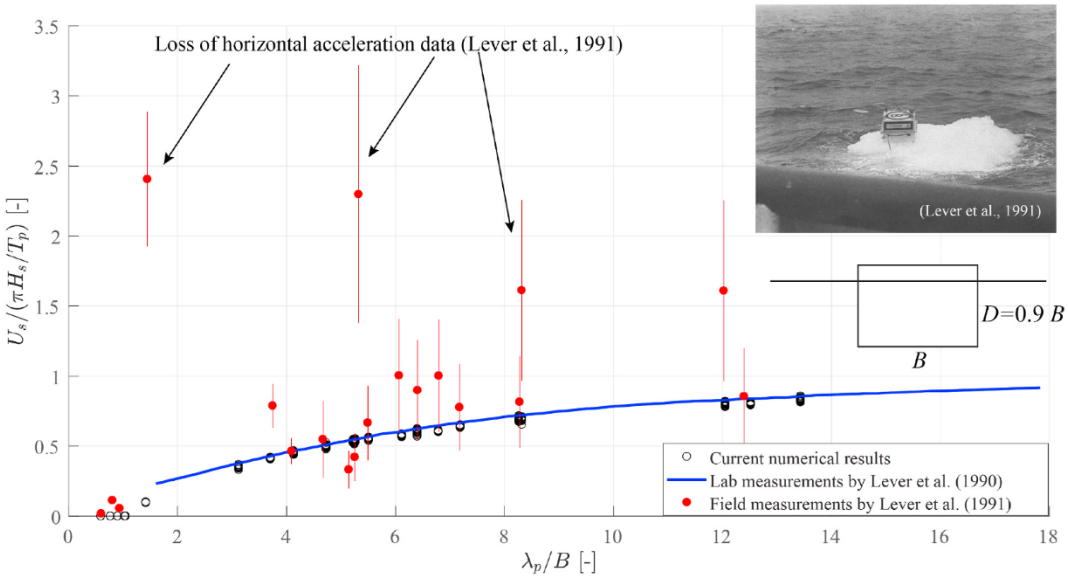

Fig. 10. Comparison of significant sway velocities for various sized glacial ice feature in various irregular wave conditions described by the JONSWAP wave spectrum with significant wave height H_s, peak wave period $T_P$and peak wave length λ_P.

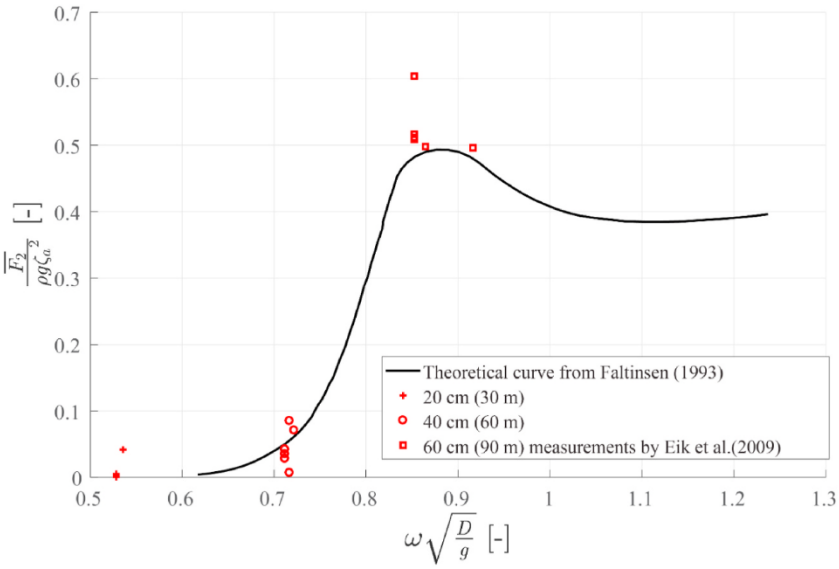

Fig. 11. Comparison of the measured slow drift force versus the theoretical curve utilised to calculate the drift motion (three sizes of cuboidal glacial ice features are tested with a scale factor of 150; model-scale sizes are presented with targeted full-scale size in brackets).

put together with the measurement error highlighted. Despite the different geometries, as commented before, most of the simulated results fall within the error ranges of the measurements.

3.3. Relative motion and impact sampling

After the introduction and validation of the methods to calculate the wave-driven oscillatory and drift motion of a glacial ice feature, the next step is to calculate the motion of the structure to establish the relative motions between the two impacting bodies. When we know the relative motion, we can sample impact events and calculate the distribution of impact location and impact velocity.

3.3.1. Structure motion

Compared with the glacial ice feature, a structure is often large and exhibits relatively smaller motion in waves. Therefore, 'linear

Table 1
Summary of all the validation cases together with the goodness of fitting between the current numerical results and existing numerical and experimental results.

Case #	Comparisons with	Features of the methods	Goodness of fitting			
			Heave		Sway	
1	RAOs calculated by commercial software	Single cubic body in regular waves without any nonlinearities	Fig. 3	$R^2 = 0.9914$	Fig. 4	$R^2 = 0.8197$
2–1	RAOs measured from laboratory tests	Single cubic body in regular waves without any nonlinearities	Fig. 5	$R^2 = 0.8007$	Fig. 6	$R^2 = 0.7272$
2–2	Laboratory-measured oscillatory motions	Single cubic body in regular waves with nonlinearities included	Fig. 7	$R^2 = 0.0068$	Fig. 8	$R^2 = 0.7115$
3	Field-measured oscillatory motions	Irregular waves, irregular geometries and nonlinearities	Fig. 9	Mostly within measurement error ranges	Fig. 10	Mostly within measurement error ranges
4	Laboratory-measured drift motion	Single cubic body in regular waves			Fig. 11	$R^2 = 0.9764$

wave theory'-based RAOs for the structure are adopted herein to characterise the motion in waves. For the structure, three degrees of freedoms (i.e., sway, heave and roll) are considered (see Fig. 2). Thus, the heave displacement induced by roll motion is accounted for. With the given RAOs in heave $H_3^S(\omega_j)$, sway $H_2^S(\omega_j)$ and roll $H_4^S(\omega_j)$, the local heave displacement $\eta_3^{ps}(t)$, sway displacement $\eta_2^{ps}(t)$ and sway velocity $\dot{\eta}_2^{ps}(t)$ can be estimated for a potential impact location '*P*' (in Fig. 2) using Eqs. (19) and (20).

$$\eta_3^{ps}(t) = \sum \left[\left| H_3^s(\omega_j) \right| \zeta_a^j \sin\left(\omega_j t - k_j x - \varphi_j\right) + L^{ps} \left| H_4^s(\omega_j) \right| \zeta_a^j \sin\left(\omega_j t - k_j x - \varphi_j\right) \right] \tag{19}$$

$$\eta_2^{ps}(t) = \sum \left[\left| H_2^S(\omega_j) \right| \zeta_a^j \cos\left(\omega_j t - k_j x - \varphi_j\right) \right] \tag{20}$$

$$\dot{\eta}_2^{ps}(t) = \sum \left[\omega_j \left| H_2^S(\omega_j) \right| \zeta_a^j \sin\left(\omega_j t - k_j x - \varphi_j\right) \right] \tag{21}$$

Only the linear oscillatory motions of the structure are calculated in the above formulation. With known structural motion, the ice structure's relative motions are obtained by superimposing both the glacial ice and structure's motion in the time domain.

3.3.2. *Impact sampling*

Based on the relative motions in the time domain, impact events are sampled for further statistical analysis. Without losing generality, we consider impacts in the sway direction (see Fig. 2), where the total relative heave displacement $\Delta\eta_{Total,3}(t)$ and total relative sway velocity $\Delta\dot{\eta}_{Total,\,2}(t)$ matter. A similar method can be applied to consider impacts in the vertical direction (e.g., impact with the pontoon of the semi-submersible).

To sample incidences of impact, we adopt the same method that was introduced by Fylling [35]. The impact scenario defined by Fylling [35] is illustrated in Fig. 12. The ship (Body A) that collides with a structure (Body B) is exhibiting both an oscillatory motion and a mean drift motion with a velocity of **V** in Fig. 12. With a high drift velocity, the middle-left plot in Fig. 12 shows the relative trajectory (heave in '**Z**' and sway in '**X**') of the two bodies; and each point on this trajectory is a potential and valid impact event. That is, each spatial position has the same likelihood to be an impact location.

With the lower drift velocity in the lower-left plot in Fig. 12, the relative trajectory of the two bodies is also oscillating back and forth. In this scenario, only the advancing motions are sampled as valid impact events (the bold black line) while the negative sway motions (the thin black line) and the shielded positive sway motions (the dashed black line) are not considered valid impact events.

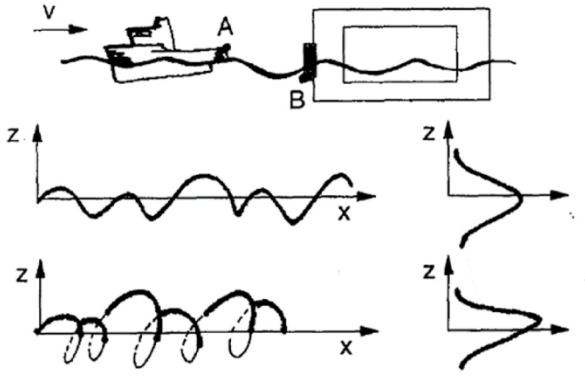

Fig. 12. For ship and installation impacts (upper plot): sampling of impact events at high current velocity (middle plot) and low current velocity (lower plot) from Fylling [35].

In both cases, impact sampling is conducted with equal spacing in the sway direction because when the ship approaches the structure, each point along the valid impact events trajectory (bold dark line) has an equal chance of impact. The implicit presupposition behind is that the influence of distance-dependent hydrodynamic effects are neglected in the sampling process. However, such a simplification is outweighed by the advantage that a large amount of impact events can be sampled from one simulation run, which is contrary to the detailed hydrodynamic analysis where we can only achieve one impact event in a single and computationally expensive simulation run [41].

Using his sampling method, the impact events tend to skew to higher locations with lower drift velocity (see the lower-right plot in Fig. 12) and the impact events are more spread with a larger drift velocity (e.g., see middle-right plot in Fig. 12).

In summary, Fylling [35] proposed two conditions to sample valid impact events out of the relative motions of the two bodies: 1) there is a positive relative velocity between the two bodies; and 2) only the non-shielded portion of track has the chance of experiencing an impact event in the space domain. That is, at the same point in the fixed space, there can only be one impact event. These conditions are implemented via a MATLAB script that calculates the relative motion and the advancing motion. Fig. 13 and Fig. 14 show an example of the calculated motion in a regular wave under the influence of a slow and large drift velocity, respectively. The sampled impact events (i.e., red markers) show that when the drift velocity is slow in Fig. 13, a significant amount of shielding occurs and most impact events are thereby skewed towards higher locations. This finding is consistent with the lower-right plot in Fig. 12 by Fylling [35].

4. Case study

Adopting the methods described in Section 3, we will carry out a case study of the impact between a 10 m wide cuboidal glacial ice feature and a semi-submersible structure. The dimensions of the ice feature are $L = 15$ m, $B = 10.3$ m and $H = 10.3$ m, which are identical to those of the studies performed by Ekeberg et al. [20] and Lu et al. [22]; which mainly used linear wave theories, and by Ommani et al. [41]; which focuses more on the nonlinearities and the near-field hydrodynamic effects (i.e., distance-dependent hydrodynamic effects were considered).

4.1. Wave conditions and simulated wave spectra

The chosen wave conditions are summarised in Table 2, which is obtained from wave contours related to the Barents Sea [36]. The respective JONSWAP wave spectra are illustrated in Fig. 15 together with the simulated spectra based on 500 wave components that each has an amplitude of $\zeta_a^j = \sqrt{2S(\omega_j)\cdot\Delta\omega}(j = 1,2,3\ \ldots.\ .500)$ and random phase angles. The agreement between assumed and simulated spectra is excellent (as expected).

4.2. Glacial ice and structure

The major input parameters are listed in Table 3. The conservative choice on the zero-frequency added mass is in accordance with the study carried out by Ommani et al. [24]; which is suitable for relatively long-duration impacts [25]; and the chosen number is also close to the measurements by Vugts [42].

For the structure, we use the same semi-submersible that was studied by Ekeberg et al. [20]. The geometry is given in Ekeberg et al. [20]. Additional parameters of the structure are listed in Table 4.

Fig. 16 visualises the simulated geometries of both the glacial ice feature and the semi-submersible. The distance between the two bodies can be arbitrary in Fig. 16, and because the hydrodynamic interaction between the two bodies are neglected and in the simulated track of the relative motion, each spatial point has an equal chance to be sampled as an impact event.

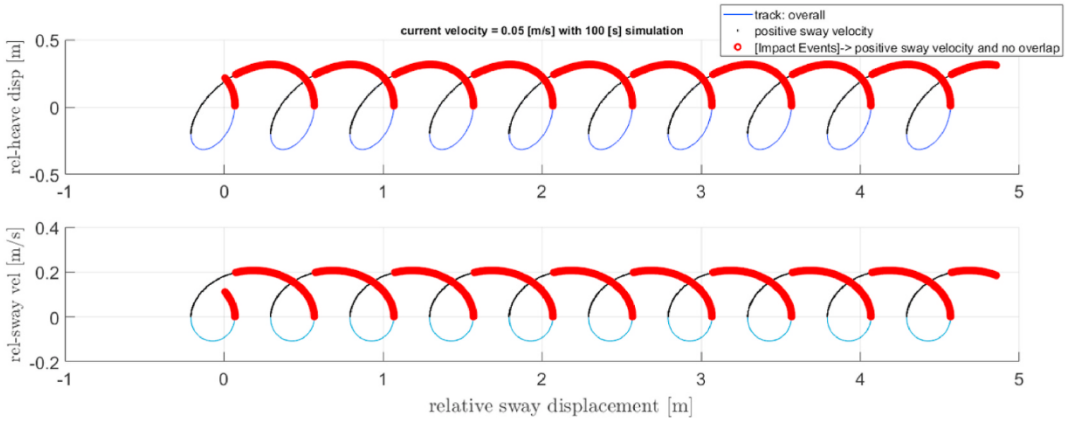

Fig. 13. One-hundred-second simulation with coupled motion track and sampled impact events under a slow drift velocity = 0.05 m/s.

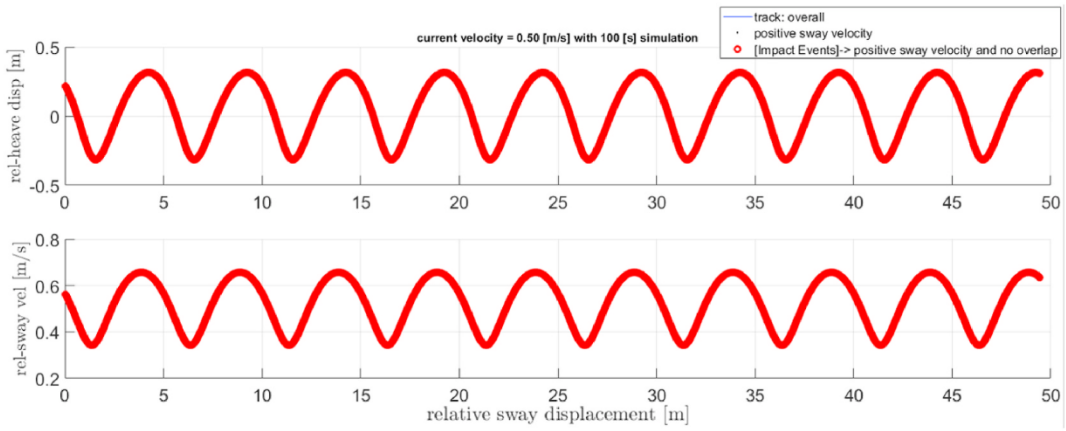

Fig. 14. One-hundred-second simulation with coupled motion track and sampled impact events under a faster current velocity = 0.5 m/s.

Table 2
Simulated wave conditions.

Wave condition	Return period of sea state [Year]	*Hs* [m]	*Tp* [s]	γ
#1	1	4.9	6.5	5
#2	1	8.6	12	2.9
#3	1	9.8	14.8	1.4
#4	100	13.8	18	1.2

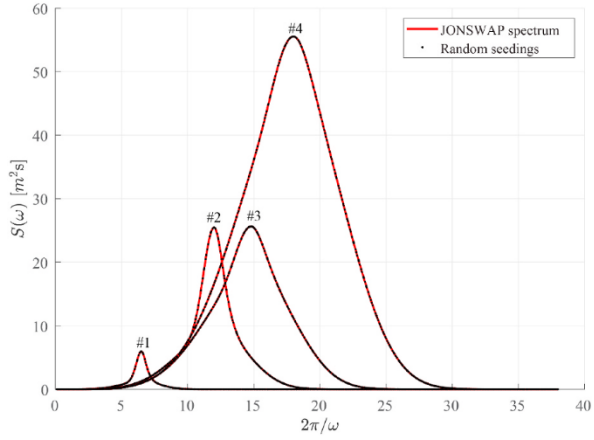

Fig. 15. Wave spectrum of the chosen wave conditions.

Table 3
Input parameters for the cuboidal glacial ice feature.

Mass M	1.43 × 103 [ton]
zero-frequency added mass in heave A_{33}	810 [ton] according to Ommani et al. [24]
zero-frequency added mass in sway A_{22}	800 [ton] according to Ommani et al. [24]
drag coefficient C_D	0.9 [-] according to Eik et al. [40]

4.3. Simulation setup

The simulation was carried out in the time domain. On the basis of the experience obtained in sensitivity studies, the total simulation time and time step $\Delta t$are set to 100,000 s and 0.1 s, respectively.

The outcome of the simulation is the distribution of impact locations and its associated impact velocities, which in turn determine

Table 4
Input parameters for the structure.

Natural period in heave T_3^c	20.8 [s]
Natural period in roll T_4^c	47.0 [s]
Arm length for heave motion correction due to roll motion L^{PS}	36.88 [m]

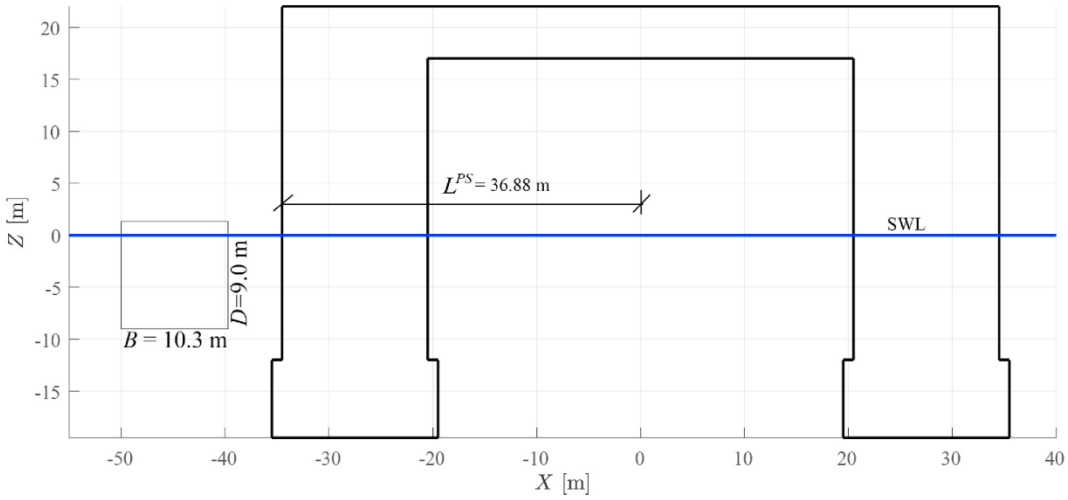

Fig. 16. Illustration of the simulated scenario; note that there is no hydrodynamic interaction between the glacial ice feature and the structure.

the kinetic energy of a given glacial ice feature for the individual impact scenarios. With known kinetic energy distributions, the structural damage can be calculated. The damage assessment is presented in the accompanying paper II.

5. Results and discussion

In our current numerical model, the wave-driven oscillatory and drift motions are calculated separately. The results and related discussions are presented sequentially in this section.

5.1. Drift motion

The drift velocities calculated in the irregular seas are presented in Table 5. As a reference, the 100-year return period water current velocity is approximately 0.79 m/s at the site where the wave conditions are chosen. Table 5 shows that most of the calculated wave-driven drift velocities according to our numerical simulation are slightly larger than the measured water current velocity, thus signifying the importance of including wave-driven motion in the analysis of the impact velocity of small glacial ice features. As expected, a higher drift velocity is attained in shorter waves.

For a large body, compared with the wave length in irregular seas (i.e., about $H_S < 0.0065B$), Eq. (22) has been proposed to calculate the drift force [32]. The associated drift velocity is presented in Table 5. As expected, the error of using this formula becomes larger as the wave length gets longer (or $T_P$gets larger), which highlights the inappropriateness of using most existing empirical formulas to calculate the drift force on a small glacial ice feature. Most of these formulas are developed for large glacial ice features (in the order of hundreds of metres). At the same time, the comparisons made in Table 5 also shows the improvement that the current study has made in calculating the drift velocity using Eqs. (15) and (17).

$$\overline{F_2} = \frac{1}{16}\rho g H_S^2 \tag{22}$$

The calculated drift velocity based on our numerical model in Table 5 shall be superimposed on the wave induced oscillatory velocity when calculating the total relative impact velocities.

5.2. Relative motions and impact events

For the purpose of illustrating the main feature of the results, we select the case in wave condition #3 with significant wave height $Hs = 9.8$ m and wave period $Tp = 14.8$ s. A sample of the simulated results for the relative heave displacement and sway velocity are presented in Fig. 17. On the overall track (blue lines), not all the motions are valid impact events. Following the method by Fylling

Table 5
Drift velocity calculated under different wave conditions.

Wave condition	*Hs* [m] *Tp* [s]		Drift velocity [m/s]	
			Current study	According Eq. (22)
#1	4.9	6.5	1.62	1.91
#2	8.6	12	1.1	3.35
#3	9.8	14.8	0.98	3.81
#4	13.8	18	0.96	5.37

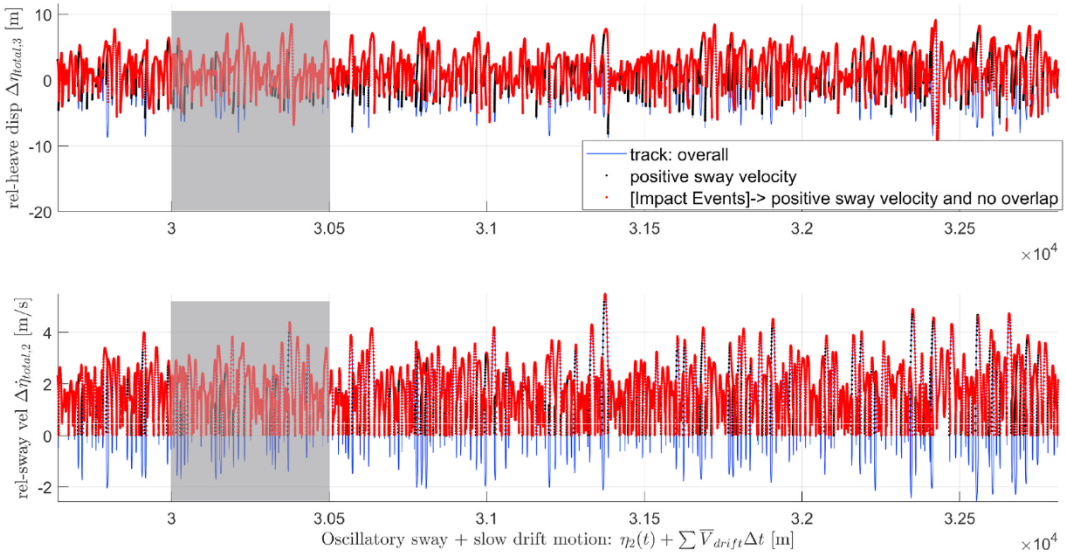

Fig. 17. Sample of simulation results 1) upper plot: the relative heave motion (i.e., rel-heave disp $\Delta\eta_{Total,3}(t)$); and 2) lower plot: the relative sway velocity (i.e., rel-sway vel $\Delta\dot{\eta}_{Total,2}(t)$).

[35]; valid impact events are resampled (red dots).

A closer view of the impact sampling procedure is presented in Fig. 18 for the shaded area in Fig. 17. The impact sampling process is shown to be effective and can record tens of thousands of impact events in one simulation run. With all of these impact events,

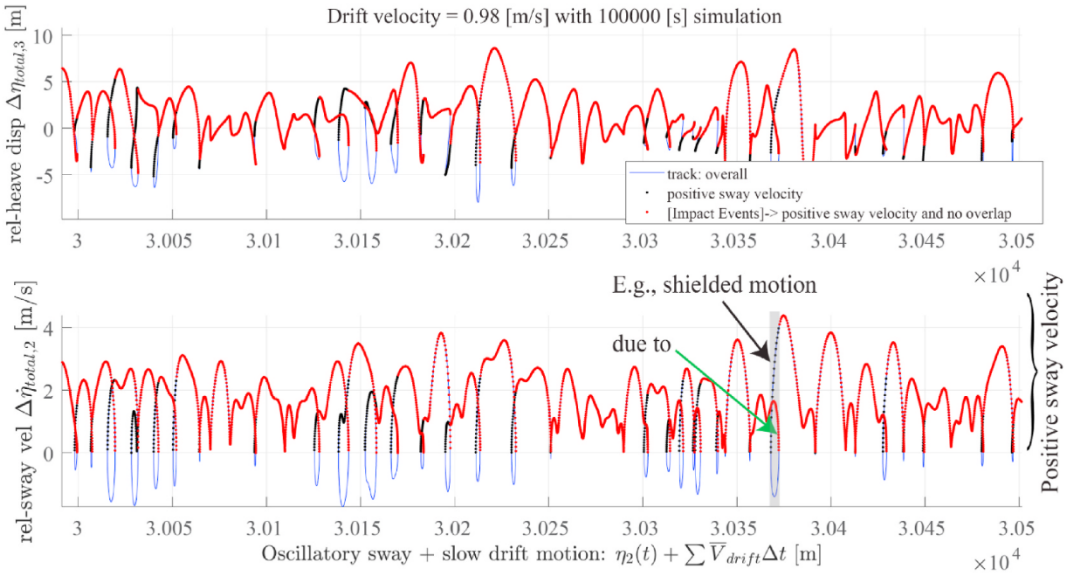

Fig. 18. Closer view of the simulated results from the shaded area in Fig. 17.

statistical information of the correlated impact height (related to $\Delta\eta_{Total,3}(t)$) and impact velocity ($\Delta\dot{\eta}_{Total,2}(t)$) can be obtained as shown in Fig. 19.

5.3. Distribution of impact height and impact velocity

With approximately 500,000 sampled impact events in Fig. 19, the probability density distributions can be fit to the impact velocity and the impact height, as shown in Fig. 20 and Fig. 21, respectively. The two-parameter Weibull distribution fits best to the impact velocity, whereas the Normal distribution fits best to the impact height. In a previous study [24,41], rather limited impacts events (i.e., approximately 20, 40 and 120 impact events) were available for fitting a Gumbel distribution; however, the current method enables a much more comprehensive and smoother statistical fitting.

Table 6 summarises the parameters of the respective best-fit distribution functions for the overall impact velocity and impact height for all cases.

The impact velocity and impact height are correlated in the time-domain simulations. The statistical distribution of the impact velocity for different heights can therefore be extracted. The results are exemplified in Fig. 22. The trend is consistent with that observed in previous studies based on linear wave theory [22,43]: a larger impact velocity is expected at high locations.

The probability distribution of impact and fractiles of the conditional impact velocity distribution at various heights are plotted with reference to the structure with the SWL in Fig. 23 and Fig. 24 for different wave conditions (i.e., a relatively long wave condition #3 and a relatively short wave condition #1 from Table 2). The plots show that for long wave conditions, the impact range is more spread compared with that of the short-wave conditions, which is also reflected by the standard deviation of the impact height σ in Table 6, i.e., a larger standard deviation is obtained for longer waves. This finding is understandable because longer waves often mean larger significant wave heights, which excite the glacial ice feature and the structure to oscillate in a much wider vertical range.

The distribution of impact velocity over the height shows a similar trend, i.e., in long waves, the velocity distribution is more dispersed, whereas in short waves, it is more concentrated. For the same exceedance level, the difference between the largest and the smallest impact velocity in Fig. 23 is more significant than that in Fig. 24. Quantitatively, in Table 6, the scale parameter a, which characterises the 'spread' of the distribution, increases with increasing wave length. In addition, the most probable impact height in Fig. 24 is much lower than that in the long wave conditions because the ice is more prone to submergence under small significant wave height conditions.

The results in Figs. 23 and 24 demonstrate the novelty of the numerical model: the distributions of the impact location and its associated impact velocity at different heights are constructed efficiently and represent key information for structural damage assessments.

5.4. Comparison with related studies

In this section, we will compare the calculated overall impact velocity and impact location with the results obtained in related studies. Key data are presented in Table 7 and Table 8.

In Table 7, the results from different projects are quite close to each other, although they are based on different methods. Study #1 was based on linear wave theory and frequency domain analyses. The calculated frequency-domain impact velocities were further processed assuming the Rayleigh distribution of 3-h maxima values. This is a rather conservative approach. Study #2 is based on linear wave theory's time domain analysis and the same Fylling's approach (1994) is adopted to derive the statistical information of impact

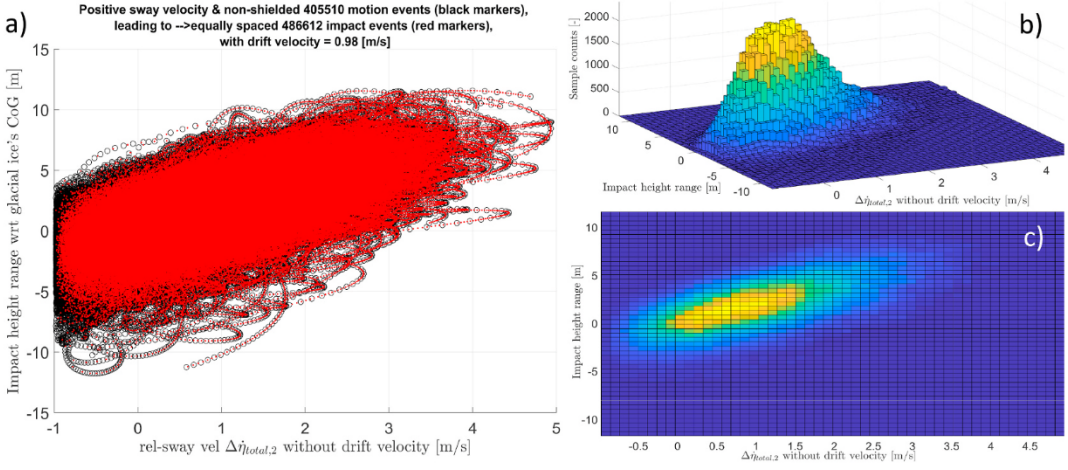

Fig. 19. Impact height versus impact velocity for the sampled impact events (red dots) for the case with $Hs = 9.8$ m and $Tp = 14.8$ s (a long wave): a) the space-equal sampling process; b) and c) the joint distribution of the sampled impact events. (For interpretation of the references to colour in this figure legend, the reader is referred to the Web version of this article.)

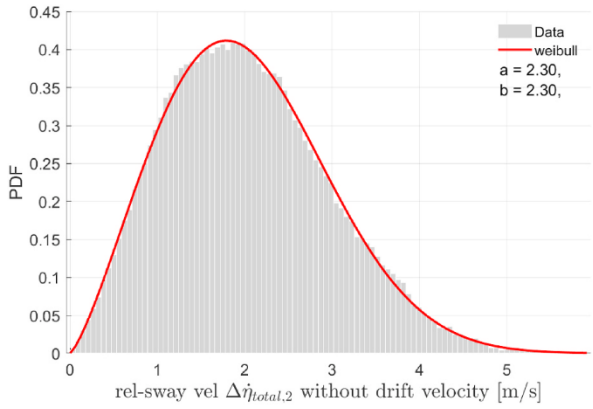

Fig. 20. Overall impact velocity distribution for the sampled impact events (red dots in Fig. 19) for wave condition #3, with $Hs = 9.8$ m and $Tp = 14.8$ s (a relatively long wave condition in Table 2). (For interpretation of the references to colour in this figure legend, the reader is referred to the Web version of this article.)

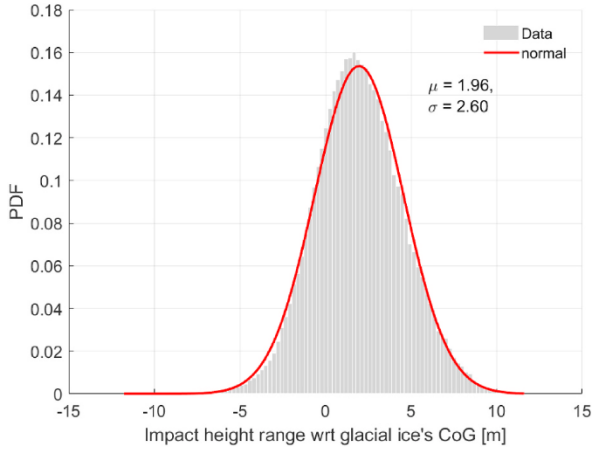

Fig. 21. Overall impact height distribution for the sampled impact events (red dots in Fig. 19) for wave condition #3, with $Hs = 9.8$ m and $Tp = 14.8$ s (a relatively long wave condition in Table 2). (For interpretation of the references to colour in this figure legend, the reader is referred to the Web version of this article.)

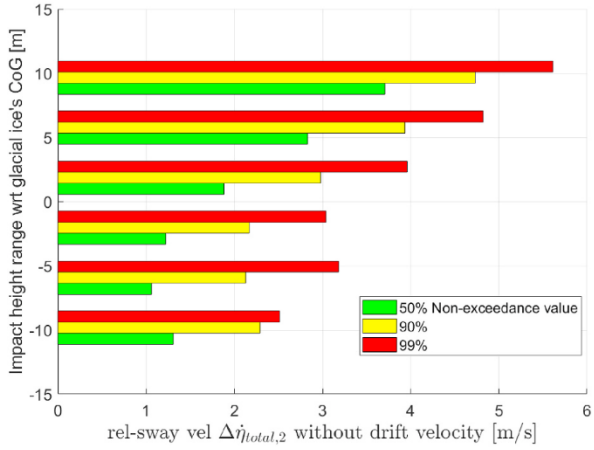

Fig. 22. Impact velocities at different heights for the glacial ice feature for the case with $Hs = 9.8$ m and $Tp = 14.8$ s (wave condition #3, with a relatively long wave).

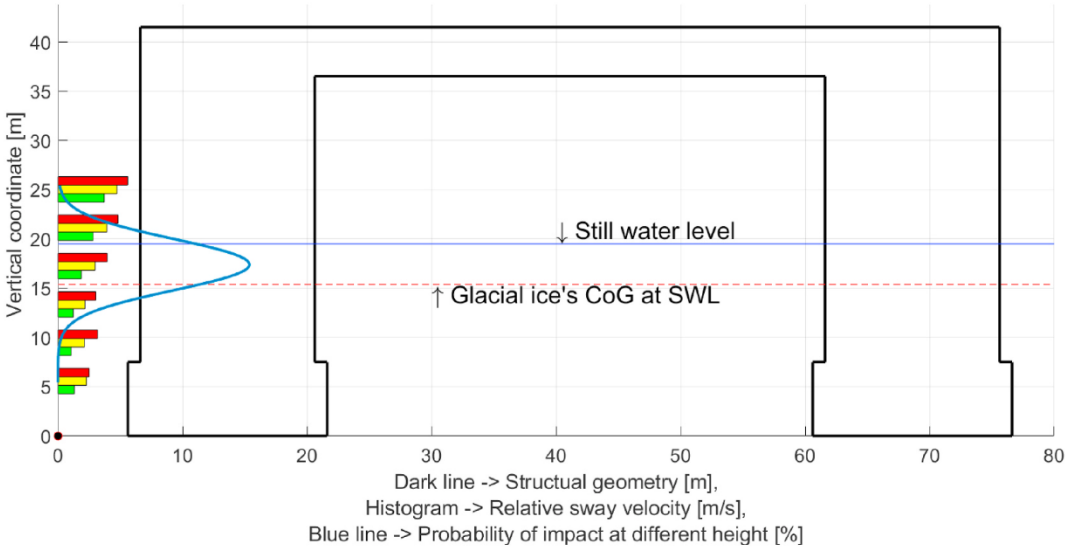

Fig. 23. Impact velocity distribution and impact probability at different heights of the structure for the case with $Hs = 9.8$ m and $Tp = 14.8$ s (i.e., a relatively long wave (wave condition #3)).

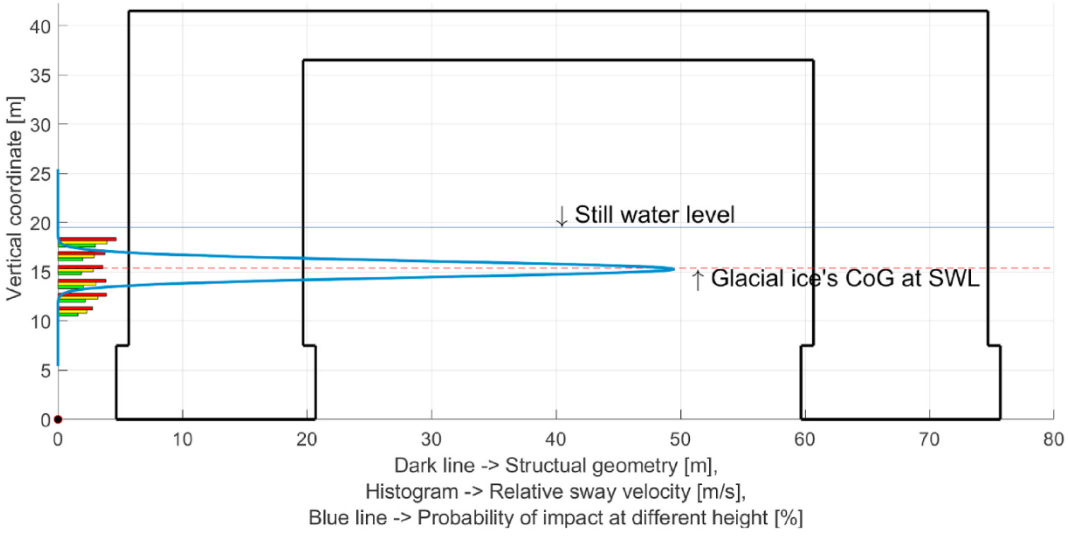

Fig. 24. Impact velocities distribution and impact probability at different height of the structure for the case with $Hs = 4.9$ m and $Tp = 6.5$ s (i.e., a relatively short wave (wave condition #1)).

velocity and heights; however, this study was conducted on a different glacial ice geometry with a much smaller size. It is only presented here as a reference. Study #3 introduced nonlinear hydrodynamic effects, but statistical information was drawn only from a handful of impact events. Therefore, despite all these differences, it is encouragingly surprising to see the calculated results are 'quite close' in Table 7.

Moreover, the current numerical model predicts smaller impact velocities and impact height ranges compared to those reported in Studies #1 for all wave conditions and in Study #3 in Wave Conditions #1 and #2. In all three studies (i.e., Studies #1, #2 and #3), a same cubical glacial ice feature were analysed. The uncertainties/conservatism of the predictions in these related studies appear to be decreasing.

More specifically, in Table 8, Study #3 performed limited impact scenarios (around 20 impacts), from which, a not-yet-converged Gumbel distribution was utilised to fit these limited data to derive a single mean value and 90% non-exceedance value with respect to the impact height. The physical meaning of the results in Table 7 for Study #3 is that: 1) the mean value represents that in average where the location of hit is; and 2) the 90% non-exceedance value represents that 90% of the hit locations are below that height.

In Studies #1, #2 and the current study, the impact height's mean and 90% non-exceedance values are presented as a range derived

Table 6
Overall impact velocity and impact height distributions[a].

Wave condition	Weibull distribution of the overall impact velocity [m/s]	Maximum likelihood estimation: parameters' range with 95% confidence
#1	$a = 2.20$; $b = 2.99$	a = [2.1951 2.1987]; b = [2.9886 2.9993]
#2	$a = 2.29$; $b = 2.32$	a = [2.2833 2.2888]; b = [2.3187 2.3283]
#3	$a = 2.30$; $b = 2.30$	a = [2.2925 2.2984]; b = [2.2906 2.3007]
#4	$a = 2.87$; $b = 2.23$	a = [2.8670 2.8755]; b = [2.2216 2.2324]
Wave condition	Normal distribution of the impact height relative to the CoG of glacial ice [m]	Maximum likelihood estimation: parameters' range with 95% confidence
#1	$\mu = -0.17$; $\sigma = 0.81$	μ = [-0.1682–0.1645]; σ = [0.8045 0.8071]
#2	$\mu = 1.40$; $\sigma = 2.34$	μ = [1.3951 1.4076]; σ = [2.3435 2.3523]
#3	$\mu = 1.96$; $\sigma = 2.60$	μ = [1.9574 1.9719]; σ = [2.5907 2.6010]
#4	$\mu = 3.39$; $\sigma = 3.79$	μ = [3.3799 3.4036]; σ = [3.7859 3.8027]

[a] a and b are the scale and shape parameters for the Weibull distribution, respectively; and μ and σ are the mean and the standard deviation for the Normal distribution, respectively.

Table 7
Overall impact velocity calculated from different studies: Study #1 [20]; Study #2: [21,22]; Study #3: [24,41].

Wave Condition	Impact Velocity [m/s]							
	Study #1		Study #2[a]		Study #3		Current Study	
	Mean	90%	Mean	90%	Mean	90%	Mean	90%
#1	2.6	2.9	NA[b]	NA	2	3.55	1.92	2.91
#2	3.5	4	NA	NA	2.25	4.01	1.95	3.27
#3	3.4	3.8	NA	NA	1.66	3.13	1.96	3.30
#4	3.9	4.4	1.8[a]	3[a]	NA	NA	2.44	4.18

[a] Results from Study #2 are calculated based on a much smaller ellipsoidal glacial ice feature, whereas the rest are based on the cuboidal glacial ice feature.
[b] NA stands for 'Not Available' and it means that the wave conditions are not analysed in pertinent studies.

Table 8
Overall impact height calculated from different studies: Study #1 [20]; Study #2: [21,22]; Study #3: [24,41].

Wave Condition	Impact Height Calculated from SWL (positive upward) [m]							
	Study #1		Study #2[a]		Study #3[b]		Current Study	
	Mean	90%	Mean	90%	Mean	90%	Mean	90%
#1	[-7.22–1.02]	[-7.62–0.62]	NA	NA	−3.58	2.29	[-4.67–3.57]	[-6.23–2.01]
#2	[-8.42 0.18]	[-8.92 0.68]	NA	NA	−2.6	4.11	[-6.0 -2.24]	[-8.62 0.38]
#3	[-9.22 0.98]	[-9.82 1.58]	NA	NA	−4.39	2.54	[-6.41–1.83]	[-9.45 1.21]
#4	[-13.12 4.88]	[-14.32 6.08]	[-4.68–1.08]	[-7.28 1.52]	NA	NA	[-7.81–0.43]	[-12.4 8.11]

[a] Results from Study #2 are calculated based on a much smaller ellipsoidal glacial ice feature, whereas the rest are based on the cuboidal glacial ice feature.
[b] The impact range in Study #3 was not presented. Instead, a single value was derived from the limited amount of impact height statistics.

from the Normal distribution. The physical meanings of these values are: 1) the mean is that 50% of the impact will fall within this range; and 2) 90% of the impact will fall within the presented ranges under 90%.

We see from Table 8 that the mean impact location from Study #3 all fall within the mean range predicted by the current study. Especially in wave condition #3, the mean of Study #3 is almost in the centre of the mean range predicted by the current study. For the wave conditions #1 and #2, although Study #3's predictions are on the edge of the current study's prediction, we tend to believe that this is caused by insufficient statistic data from Study #3. With regard to the 90% non-exceedance values, we see that Study #3 predicts rather conservative upper-limit impact height encompassing all the predicted ranges given in both Study #1 and the current study. Bearing in mind that Study #1 adopted the 3-h maxima values to conduct its statistical analyses, which is already a rather conservative assumption; yet Study #3 yields even more conservative 90% non-exceedance impact heights, signifying the importance of having sufficient impact events from which a proper statistical distribution can be drawn.

6. Further discussions

6.1. The near-field hydrodynamic simplifications

The simplified numerical model presented in this paper is based the assumption of ignoring the near-field hydrodynamic effects. Most physical experimental results indicate that there is an impact velocity reduction as a glacial ice feature approaching a large structure. This phenomenon is reflected by the following experimental observations: e.g., 1) the existence a repulsive force [28]; 2) a cushioning effect for a bergy-bit with the presence of Tera Nova FPSO [44]; 3) when a tanker is passing by, without collision, the sway motion of a nearby iceberg increases if there are waves (i.e., the iceberg is further pushed away from the passing-by tanker) [45]; 4) the measured velocity reduction of around >10% by Ref. [25] and around 10%–40% reduction by Mak et al. [46] for an iceberg approaching a large structure. At the same time, theoretical calculations show that there is an increase in added mass as the gap distance between the glacial ice feature and the structure decreases. In a similar problem, Study #3 [24,41] shows that the added mass in the sway direction increases 47% comparing to its far-field value. Given the decreased impact velocity (i.e., 10%–40% reduction) and increased added mass (i.e., 47% increase), following Eq. (1), we can calculate that the kinetic energy ignoring near-field effects is about 1.05–2.38 times of that considering the near-field hydrodynamic effects. Moreover, based on our initial assessment of the simulation results from Study #3, the difference is closer to the lower bound (i.e., 1.05). Thus, in its totality, the proposed numerical model is predicting a relatively conservative impact kinetic energy.

As discussed in the introduction section, performing accurate near-field hydrodynamic analysis is not the intention of this paper. This paper aims to make fit-for-purpose hydrodynamic simplifications to achieve the construction of impact kinetic energy in accordance to the standard. In order to accurately capture the near-field hydrodynamic effect, we believe that experiments are the only viable options nowadays. However, it may be unrealistic at the current stage to rely purely on physical model tests to construct, e.g., the 10^{-2} or 10^{-4} design kinetic energy, which often requires a large amount of impact events under different wave conditions to draw the statistical information from. A more viable approach to address this issue might be to make a synergy among 'physical model tests', 'detailed numerical analysis', and 'simplified numerical model (e.g., the model presented in this study)'. Some physically informed parameterisations can be developed/introduced (based on detailed numerical analyses and physical model tests) to enrich the simplified numerical model such that it can take into account the near-field hydrodynamic effects to certain extend yielding an even better prediction. However, this is beyond the scope of this paper and is thus left out for future work.

6.2. Kinetic energy of impact

Table 7 shows the 90% non-exceedance overall impact velocity of the 10 m wide glacial ice feature in wave conditions with different return periods. Ideally, the calculations should be repeated according to the probabilistic framework described in Section 2.1 for various sizes of glacial ice features and different wave conditions to construct the distribution of the kinetic energy $F_V(E_k)$. Thereafter, the cumulative distribution function $F_Z(E_k)$ of the annual maxima E_k^Z might be calculated by Eq. (2) with a given encounter frequency E_N. With known $F_Z(E_k)$, the design kinetic energy $E_{k,E}^{design}$ might be obtained through Eqs. (3) and (4) for specific structures. Here, we will only examine the kinetic energy for this particular impact event (i.e., the impact from a 10 m wide glacial ice feature on a given structure). The encounter frequency in the Barents Sea is associated with a large uncertainty and may be in the range of 10^{-2} to 10^{-4} per year [36]. Suppose the encounter frequency is 10^{-3} per year; to achieve a design kinetic energy with a probability of 10^{-4} per year (or an exceedance level of 0.9999 in Eq. (4)), we should most likely choose the one-year return wave condition #3 with the 90% non-exceedance impact velocity to estimate the corresponding impact energy, which leads to an impact energy of approximately 12 MJ for this impact scenario based on Eq. (1). This value will be used as a characteristic impact energy in the structural damage assessment in the accompanying Paper II.

7. Conclusions

The glacial ice features in the northern and central Barents Sea may threaten ships and offshore structures. Particularly, small glacial ice features, which are difficult to detect and manage by concurrent technologies, are of concern. Given the need to study the impacts from small glacial ice features on a structure, we developed a numerical model that is capable of 1) efficiently simulating the relative motion between the two impacting bodies without sacrificing important nonlinear features, such as submergence of small glacial ice features in waves; and 2) sampling sufficient impact events to draw statistical information, such as the impact locations (or probability) and their associated impact velocities.

For the calculations of relative motion, focus was placed on developing algorithms to determine the wave-driven oscillatory and drift motion of the glacial ice features, which were calculated separately and reasonably validated against existing numerical and experimental results. The method originally developed by Fylling [35] was adopted to sample sufficient impact events (on the order of 500,000 events) from the superimposed relative motion track calculated previously. For each impact event, the correlated impact location and impact velocity were available and showed the following statistical trends:

- The overall impact location and impact velocities can be described by the Normal and Weibull distributions, respectively;
- The impact velocity increases with increasing impact height and higher sea states;

- Under longer/higher wave conditions, the impact height range is more dispersed, whereas under shorter wave conditions, the impact height range is more concentrated;
- Under shorter wave conditions, the most probable impact height is below the Centre of Gravity (CoG) of the glacial ice feature in still water, indicating that the submergence of ice occurs more frequently for shorter waves than longer waves.

It is worth mentioning that in our model, we have neglected the near-field hydrodynamic effects from the structure to the approaching small glacial ice feature for practical and fit-for-purpose reasons, i.e., to be able to efficiently sample a large amount of impact events from which we can draw statistical information regarding the impact location and impact velocities. Perhaps a more complete study that includes 1) a comprehensive impact analysis with certain hydrodynamic interaction simplifications (as conducted in the current paper); and 2) selected cases with more detailed hydrodynamic treatment (e.g., as conducted by Ref. [24,41]) and relevant physical model tests could yield a more precise answer. Our initial calculations and assessment with existing numerical and experimental results indicate that our predictions are slightly on the conservative side with such simplification (see Section 6.1). Moreover, as indicated by the comparison presented in Tables 7 and 8, the results from the different studies are rather close despite the use of different methods with various levels of hydrodynamic simplifications. This finding supports the quantitative results obtained in the case study of the impact between the 10 m wide glacial ice feature and the selected structure. The proposed numerical model can be efficiently utilised to calculate the impact velocities for a large amount of impact scenarios for a given distribution of glacial ice feature sizes and wave conditions, which will enable us to follow the probabilistic framework stated in ISO19906 [3] for the quantification of the design kinetic energy. This work will constitute the basis of the detailed structural damage assessment (as described in the accompanying Paper II).

Declaration of competing interest

The authors declare no conflicts of interest.

Acknowledgements

The authors would like to thank the financial sponsorship from the Petroleum Safety Authority Norway (Ptil: Petroleumstilsynet) to carry out this study. The first author would also like to thank VISTA, which is a basic research programme in collaboration between the Norwegian Academy of Science and Letters and Equinor (former Statoil), for financial support in writing this paper. The work by the second and third authors was supported by the Research Council of Norway through the Centres of Excellence funding scheme, project number 223254 – NTNU AMOS.

Appendix A

A comparison of the slow drift force calculation in the frequency domain is presented in Fig. 25, in which the dark curve represents the results calculated by the method presented in Section 3.2.1 and the blue square markers show the complete solutions from Faltinsen [32]. The dark curve underestimates the drift force for short waves and overestimates it for long waves. To explain this discrepancy, we consider two extreme scenarios when calculating the slow drift force by the method presented in Section 3.2.1.

First, the slow drift force $\overline{F}_2$ is formulated in Eq. (23) for a regular wave and scaled with the square of the reflected wave height A_R [47]. In extremely short wave conditions (i.e., ω is large in Fig. 25), the reflected wave height can be approximated by the incoming incident wave amplitude, i.e., ζ_a. However, as we have adopted the undisturbed wave potential in our formulation of the Froude-Krylov force, there are no reflected waves ($A_R = 0$), which explains the nearly zero drift force for short waves in our numerical model in Fig. 25.

$$\overline{F}_2 = \frac{\rho g}{2} A_R^2 \tag{23}$$

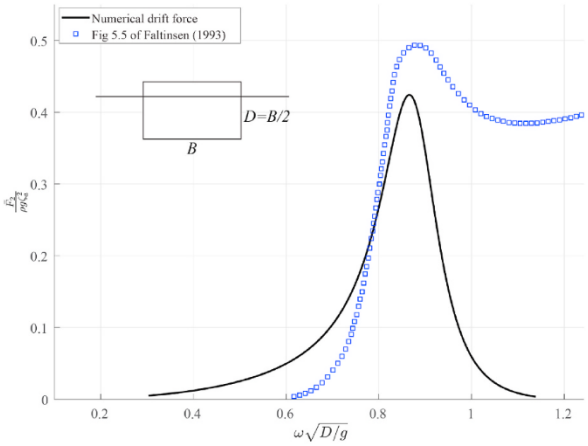

Fig. 25. Slow drift force comparisons ($A_{33} = 0.29M$ according to the original graph).

Second, although the incident wave potential is a good approximation of the total potential for long waves, the calculation of drift force requires integrating the exact wetted surface using the complete pressure given in Eq. (24) according to the direct pressure integration method [32]. However, in our formulation of dynamic pressure in Eq. (8), the 3rd term in Eq. (24) is not included. Only the first two parts of the pressure terms are integrated over the instantaneous wetted surface: 1) the first term is the restoring force term in Eq. (12) excluding the gravity part; and 2) the second term is the Froude-Krylov force term in Eqs. (7) and (8). This integration explains the overestimation the drift force for long waves.

$$p = -\rho g z - \rho\frac{\partial\varphi}{\partial t} - \frac{\rho}{2}\left[\left(\frac{\partial\varphi}{\partial y}\right)^2 + \left(\frac{\partial\varphi}{\partial z}\right)^2\right] \tag{24}$$

In summary, the formulations introduced in Section 3.2.1 are not sufficient to characterise the complete slow drift motion of small glacial ice features. Therefore, any slow drift motion calculated by the formulation shall be filtered away, leaving only the oscillatory components.

References

[1] Monteban D, Lubbad R, Samardzija I, Løset S. Enhanced iceberg drift modelling in the Barents Sea with estimates of the release rates and size characteristics at the major glacial sources using Sentinel-1 and Sentinel-2. Cold Reg Sci Technol 2020;175:103084.
[2] Yu Z, Lu W, Van Den Berg M, Amdahl J, Løset S. Glacial Ice Impacts, Part II: damage assessment and ice-structure interactions in accidental limit states (ALS). 2020 [Submitted to) Marine Structures].
[3] ISO19906. Petroleum and natural gas industries - Arctic offshore structures,International Standard. Geneva, Switzerland: International Standardization organization; 2019.
[4] Spring W. Ice data acquisition – summary report. Mobil Research Dev. Corp., Dallas E&P Eng.; 1994. p. 90.
[5] Spring W, Vinje T, Jensen H. Iceberg and sea ice data obtained in the annual expeditions of the Barents Sea ice data acquisition Program (IDAP). In: Proceedings of 12th international conference on port and ocean engineering under arctic conditions; 1993. p. 17–20.
[6] Mcclintock J, Bullock T, Mckenna R, Ralph F, Brown R. Greenland iceberg management: implications for grand banks management systems. PERD/CHC Report; 2002. p. 20–65.
[7] Mcclintock J, Mckenna R, Woodworth-Lynas C. Grand banks iceberg management. PERD/CHC report 20-84. Report prepared by AMEC Earth & Environmental, St. John's, NL, RF McKenna & Associates. NL: Wakefield, QC, and PETRA International Ltd Cupids; 2007.
[8] Eik K. Review of experiences within ice and iceberg management. J Navig 2008;61:557–72.
[9] Rossiter JR, Guigné J, Hill C, Pilkington R, Reimer E, Ryan J, Wright B. Remote sensing ice detection capabilities - east coast. Environmental Studies Research Funds; 1995.
[10] O'connell B. Marine radar for improved ice detection. In: Proceedings of the 8th international conference and exhibition on performance of ships and structures in ice, 20–23 july 2008, banff, alberta, Canada; 2008 [Citeseer].
[11] Sayeed T, Colbourne B, Quinton B, Molyneux D, Peng H, Spencer D. A review of iceberg and bergy bit hydrodynamic interaction with offshore structures. Cold Reg Sci Technol 2017;135:34–50.
[12] Mountain DG. On predicting iceberg drift. Cold Reg Sci Technol 1980;1:273–82.
[13] Sodhi D, El-Tahan M. Prediction of an iceberg drift trajectory during a storm. Ann Glaciol 1980;1:77–82.
[14] Hsiung CC, Aboul-Azm AF. Iceberg drift affected by wave action. Ocean Eng 1982;9:433–9.
[15] Carrieres T, Sayed MA, Savage S, Crocker G. Preliminary verification of an operational iceberg drift model. Proc - Int Conf Port Ocean Eng under Arct Cond 2001.
[16] Kubat I, Sayed M, Savage SB, Carrieres T. An operational model of iceberg drift. Int J Offshore Polar Eng 2005;15.
[17] Arunachalam VM, Murray JJ, Muggeridge DB. Short term motion analysis of icebergs in linear waves. Cold Reg Sci Technol 1987;13:247–58.
[18] Sen D. Prediction of wave loads and motions of floating marine structures by three-dimensional flow theory. Memorial University of Newfoundland; 1983.
[19] Lever JH, Attwood D, Sen D. Factors affecting the prediction of wave-induced iceberg motion. Cold Reg Sci Technol 1988;15:177–90.
[20] Ekeberg O-C, Shipilova O, Birknes-Berg J, Johansen A. Glacial ice impact. In: Petroleumstilsynet, editor. *PTIL-Konstruksjonssikkerhet i nordområdene*. Stavanger, Norway: DNV GL AS oil & gas environmental loading & Response; 2018.
[21] Lu W, Amdahl J. Glacial ice and offshore structure impacts under wave and current excitation. In: Proceedings - international conference on port and ocean engineering under arctic conditions 2019 delft, The Netherlands; 2019.

[22] Lu W, Yu Z, Van Den Berg M, Lubbad R, Amdahl J, Løset S, Kim E. Assessment of structural damage due to glacial ice impact. In: Petroleumstilsynet, editor. *PTIL-Konstruksjonssikkerhet i nordområdene.* Stavanger: Petroleumstilsynet; 2018.
[23] Isaacson M, Stritto F. Motion of an ice mass near a large offshore structure. Offshore Technology Conference. Offshore Technology Conference; 1986.
[24] Ommani B, Berthelsen PA, Firoozkoohi R. Ptil – NORD ST20_2018 Loads, design and operation of floaters in the Arctic. 2018.
[25] Isaacson M, Mctaggart K. Influence of hydrodynamic effects on iceberg collisions. Can J Civ Eng 1990;17:329–37.
[26] Isaacson M, Cheung KF. Influence of added mass on ice impacts. Can J Civ Eng 1988;15:698–708.
[27] Tsarau A, Lubbad R, Løset S. A numerical model for simulation of the hydrodynamic interactions between a marine floater and fragmented sea ice. Cold Reg Sci Technol 2014;103:1–14.
[28] Kazi IH, Chwang AT, Yates GT. Hydrodynamic interaction between a fixed and a floating cylinder. Int J Offshore Polar Eng 1998;8:5.
[29] Norsok. Actions and action effects, N-003. Oslo: Norwegian Technology Standards Institution; 2017.
[30] Fuglem M, Jordaan I, Crocker G, Cammaert G, Berry B. Environmental factors in iceberg collision risks for floating systems. Cold Reg Sci Technol 1996;24:251–61.
[31] Lever J, Colbourne B, Mak L. Model study of the wave-driven impact of bergy bits with a semi-submersible platform. J Offshore Mech Arctic Eng 1990;112:313–22.
[32] Faltinsen OM. Sea loads on ships and offshore structures. Cambridge Univ Pr; 1993.
[33] Cook RD, Malkus DS, Plesha ME, Witt RJ. Concepts and applications of finite element analysis. John Wiley & Sons; 2007.
[34] Isaacson M, Mctaggart KA. Modelling of iceberg drift motions near a large offshore structure. Cold Reg Sci Technol 1990;19:47–58.
[35] Fylling I. On the statistics of impact velocities and hit positions related to collisions and mating operations for offshore structures. In: BOSS conference). BOSS; 1994. p. 297–306.
[36] Dezecot C, Eik KJ. Barents Sea east blocks metocean design basis "fysisk miljø i barentshavet sørøst,". 2015.
[37] Dnvgl. SESAM user manual WADAM - wave analysis by diffraction and Morison theory. 2017.
[38] Lever J, Klein K, Mitchell D, Diemand D. Wave-induced iceberg motion. Cold Reg Sci Technol 1991;20:11–23.
[39] Lever J, Sen D, Attwood D. The influence of shape on iceberg wave-induced velocity statistics. J Offshore Mech Arctic Eng 1990;112:263–9.
[40] Eik K, Marchenko A, Løset S. Wave drift force on icebergs–tank model tests. Proc - Int Conf Port Ocean Eng under Arct Cond 2009.
[41] Ommani B, Berthelsen PA, Lie H, Aksnes V, Løland G. Hydrodynamic modelling and estimating Response of glacial ice near a drilling rig. ASME 2019 38th international conference on ocean, offshore and arctic engineering. American Society of Mechanical Engineers Digital Collection; 2019.
[42] Vugts JH. The hydrodynamic coefficients for swaying, heaving and rolling cylinders in a free surface. Int Shipbuild Prog 1968;15:251–76.
[43] Lu W, Yu Z, Lubbad R, Amdahl J, Løset S, Kim E. Glacial ice actions: executive summary of NORD ST20 2019/313 and NORD ST19. *ST20_2019/313_Extension.* Stavanger: Petroleumstilsynet. 2019 [Petroleum Safety Authority Norway].
[44] Duggal AS, Heyl CN, Poranski PF. Terra Nova FPSO: integration of model tests and global analysis. In: The tenth international offshore and polar engineering conference. Seattle, Washington, USA: International Society of Offshore and Polar Engineers; 2000.
[45] Gagnon R. Physical model experiments to assess the hydrodynamic interaction between floating glacial ice masses and a transiting tanker. J Offshore Mech Arctic Eng 2005;126:297–309.
[46] Mak LM, Lever JH, Hinchey MJ, Duthinh D. Wave-induced bergy bit motionnear a floating oil production platform. Proceedings of the 9th International Conference on Offshore Mechanics and Arctic Engineering 1990:205–15.
[47] Maruo H. The drift on a body floating in waves. J Ship Res 1960;4:1–10.